Determination of the inclusive $(\overrightarrow{p}, \alpha)$ analyzing powers in the investigation of the ^{40}Ca$(\overrightarrow{p}, p\alpha)$ reaction with 100 MeV polarized protons

by

Tsepiso Emily Lakaje

Dissertation presented in fulfillment of the requirements for the degree of

Master of Science

to the

Department of Physics

University of Zululand

Supervisor: Dr. R. Neveling, iThemba LABS

Co-supervisor: Prof O.M. Ndwandwe, Department of Physics, University of Zululand

December 2005

Declaration

I, the undersigned, hereby declare that the work contained in this dissertation is my own original work and that I have not previously in its entirety or in part submitted it at any university for a degree.

Signature

20/04/06

Date

Abstract

Determination of the inclusive $(\overrightarrow{p}, \alpha)$ analyzing powers in the investigation of the $^{40}Ca(\overrightarrow{p}, p\alpha)$ reaction with 100 MeV polarized protons

Tsepiso Emily Lakaje
University of Zululand
December 2005

Alpha particle formation in the ^{40}Ca nucleus was investigated by means of the $(\overrightarrow{p}, p\alpha)$ reaction with a 100 MeV polarized proton beam. Coincident and singles analyzing power data were acquired for three different quasi-free angle pairs. The knocked out α particles were measured using a silicon detector telescope and the protons were measured using a K600 magnetic spectrometer. Only the singles analyzing power data for the silicon detector telescope were analyzed in this thesis. This data served as an important consistency check for the coincident results between different datasets, and it was also used in the investigation of the clustering phenomenon.

The experimental analyzing power results were compared with the theoretical calculations which were done using the THREEDEE computer code. This computer code is based on the Distorted Wave Impulse Approximation (DWIA). Experimental analyzing power results are not in good agreement with the theoretical analyzing power results.

Acknowledgements

• I thank GOD for bringing me this far because it has not been a simple ride, but He made it possible.

• My best gratitude goes to my supervisor (the best ever), Dr. R. Neveling for his guidance and unfailing support through out the duration of this project. I consider myself privileged to have been working with him.

• I wish to express my sincere gratitude to my co-supervisor Prof. O.M. Ndwandwe for his guidance and for seeing the potential in me and securing my financial assistance.

I am thankful to:

• Dr. S.V Förstch who was never too busy to help. It was wonderful working with him.

• R. Neveling, S.V Förstch, F.D. Smit, H Fujita, N. Botha, G. Hillhouse, B. Van der Ventel, S. Ntshangase, J. Mudau, J. van der Merwe, D. van Niekerk and S. Wyngaard for their help in running the experiment.

• the NRF and iThemba LABS for their financial support.

• the MANUS/MATSCI co-ordinators Drs. T.K. Marais, C. Theron, Profs. O.M. Ndwandwe and J.F. Sharpey-Schafer for making sure that everything goes accordingly.

• Special thanks to my friends including the iThemba LABS Prayer Group and Restoration Life Ministry members for their moral support.

• I am grateful to Dr. C. Pienaar , Dr. W. Pienaar and Joe Ncha for their love and courage. For always making sure that I am ready to start each week ready for work.

• M. Masikhwa, J. Mudau, N. Botha and MANUS/MATSCI students, thank you for being good and supportive colleagues.

• My last words of thanks goes to the people who are occupying a very special space in my heart: my parents (Elliot and Maletsatsi Lakaje) to whom I dedicate this thesis. I

am here today because of your love, courage and support. May the Lord bless and keep them. Not forgetting the wonderful brothers and sisters I have. Thank You!!!

Contents

Chapter 1

Introduction

1.1 Overview

In this chapter the concept of clustering will be introduced and knockout reactions as relevant to the field of nuclear physics will be described. This is followed by a short description of the previous work that was done concerning inclusive $(\vec{p}, \alpha)$ measurements. Finally the aim of the study is described.

1.2 Clustering Phenomena

A cluster can be defined as a unit that is composed of strongly correlated nucleons [Hod03]. Such clusters can take part in nuclear reactions and their properties can be studied. An example is when 2 protons and 2 neutrons come together to form an α cluster. Formation of other clusters is also possible depending on their stability, but α particle formation is quite likely because of its spin and isospin symmetry and hence its high binding energy [Hod97]. An example of other types of clusters are deuteron clusters as seen in $(p,^3\mathrm{He})$ reactions, which shows special features such as pickup and knockout processes and other successive steps in the reaction.

In the field of nuclear physics there is a long standing interest in the existence of multinucleon clusters that are found in nuclei. The tendency of some heavy unstable nuclei to emit multi nucleon clusters such as α particles led scientists in the early twentieth century to speculate on the existence of pre-formed α particles inside the decaying nucleus [Car84].

A very strong indication for the presence of clusters inside nuclei was revealed in the 1970's by quasi-free scattering at high energies. Studies of the interaction of 800 MeV protons with a range of nuclei showed peaks in the cross-section that seemed as if the protons were scattered by α and by deuteron clusters [Chr78]. Also, nuclear emulsion studies in 1950's provided proof for the existence of clusters in nuclei [Car84]. Energy and angular distributions of emitted α particles differed significantly from those expected from the statistical theory on nuclear disintegration. This difference of α's emitted when protons with energies from $\sim$ 40 MeV to 600 MeV impinge on light and heavy nuclei implied direct quasifree collisions between incident protons and α clusters in the target nucleus.

These days the formation of α clusters is mainly investigated either by α transfer reactions or by α knockout reactions. A *transfer reaction* is a reaction where a particle is transferred from the incident projectile to a target nucleus, or vice versa. It has a two-particle final state. In a *knockout reaction* a particle is removed from the target by the incident projectile. It has a three-particle final state, as shown in the α knockout reaction below:

$$p + {}^{A}_{Z}X \rightarrow p + \alpha + {}^{A-4}_{Z-2}Y \ . \tag{1.1}$$

This study is only concerned with knockout reactions. Knockout experiments are typically set up kinematically so that the momentum of the residual target is zero or very close to zero, i.e. the detectors are positioned such that they can only observe those protons and α's that originate from the nuclear reaction where the residual nucleus ${}^{A-4}_{Z-2}Y$ is stationary. The momentum of the incident particle is then mostly divided between the scattered particle and the knockout particle. This kinematic condition is referred to as the quasi-free point, and is the kinematic condition that best resembles the reaction between an incident particle and a free cluster:

$$p + \alpha \rightarrow p + \alpha \ . \tag{1.2}$$

Quasi-free scattering refers to a nuclear reaction process in which a medium energy particle knocks a particle out of a nucleus in such a way that no other violent interactions occur between the nucleus and the incident or two outgoing particles [Jac66]. For this kind of an interaction, incoming protons of energies in the range of 100 MeV to 1000 MeV are needed [Jac66]. An example of such a reaction is the ^{40}Ca$(\vec{p},p\alpha)$. In this case a proton knocks an alpha particle out of the ^{40}Ca nucleus to produce the residual target ^{36}Ar.

1.3 Knockout Reactions

Cluster knockout depends on the probability of nucleons forming clusters in a nucleus and also on the momentum distribution of the clusters [Hod03]. In a study done by Brink and Castro [Bri73] it was found that the nucleons concentrate into α particles when the density falls to about a third of the central nuclear density, thus it was suggested that in the region of the nuclear surface the formation of α particles is favoured.

The $(\vec{p},p\alpha)$ quasi-free scattering reaction at energies between 100 MeV and 296 MeV has been used to extensively study the alpha cluster structure of the ground state wave function of light nuclei such as ^{6}Li, ^{7}Li, ^{9}Be and ^{12}C [Roo77, Nad80, Wan85, Nad89, Yos98]. Theoretical calculations and experimental energy sharing cross-section data from these studies were in good agreement and it was therefore concluded that the reaction is largely a quasi-free process.

In general a more stringent test of the reaction dynamics is the ability to reproduce the spin transfer observable analyzing powers (A_y). Due to the well known spin dependence of the nuclear reaction between the proton projectile and the target, the cross-section will depend on the direction of spin of the incident proton. This is characterized by the so-called analyzing power, which is the ratio of the difference in cross-section for the projectile protons polarized upwards and polarized downwards, divided by the sum of these cross-sections. It is defined as follows:

$$A_y = \frac{1}{p}\frac{C^{\uparrow} - C^{\downarrow}}{C^{\uparrow} + C^{\downarrow}}, \tag{1.3}$$

where

$$p = p^{\uparrow} = p^{\downarrow} \tag{1.4}$$

$p^{\uparrow}(^{\downarrow})$ represents the degree of polarization for the upwards (downwards) polarized beam, and $C^{\uparrow}$ ($C^{\downarrow}$) represents the total number of events per energy bin for the proton beam polarized in the upwards (downwards) direction.

Not a lot of data is available for analyzing power measurements of the $(\overrightarrow{p}, p\alpha)$ reaction. In the study for the ^{9}Be$(p, p\alpha)$ reaction at 150 MeV, Wang *et al.* [Wan85] stated that the energy sharing analyzing power distribution agrees reasonably well with theoretical calculations. Also, Yoshimura *et al.* [Yos98] studied $(\overrightarrow{p}, p\alpha)$ reaction at 296 MeV for the targets ^{6}Li, ^{7}Li, and ^{9}Be and it was found that energy sharing analyzing power distributions are reproduced fairly well. These two studies showed that there is little input from multistep processes and they confirmed that the reaction is a quasi-free process.

Only cross section data is available on the investigation of alpha particle clustering in heavier nuclei by means of proton induced quasi-free cluster knockout. A range of target nuclei heavier than ^{12}C, namely ^{16}O, ^{20}Ne, ^{24}Mg, ^{28}Si, ^{32}S, ^{40}Ca, ^{48}Ti, ^{54}Fe and ^{66}Zn were used to investigate the ground state $(p, p\alpha)$ reaction at quasi-free kinematics by Carey *et al.* [Car84]. For this study theoretical calculations agree fairly well with the experimental energy sharing cross section distributions.

If the quasi-free knockout reaction mechanism represents a good approximation of the reaction, the analyzing power at the quasi-free point should correspond to free p-α elastic scattering data. Wang *et al.* [Wan85] showed that the analyzing power distributions of the ^{9}Be$(p, p\alpha)^{5}$He cluster knockout reaction at 150 MeV are qualitatively in agreement with free p-α elastic scattering results. This is shown in Fig. (1.1).

In addition to the above mentioned exclusive measurements, inclusive $(\overrightarrow{p}, \alpha)$ measurements where only the α particle is detected can also be used as a different way of

investigating clustering phenomenon. Inclusive $(\vec{p}, \alpha)$ measurements are discussed in the next section.

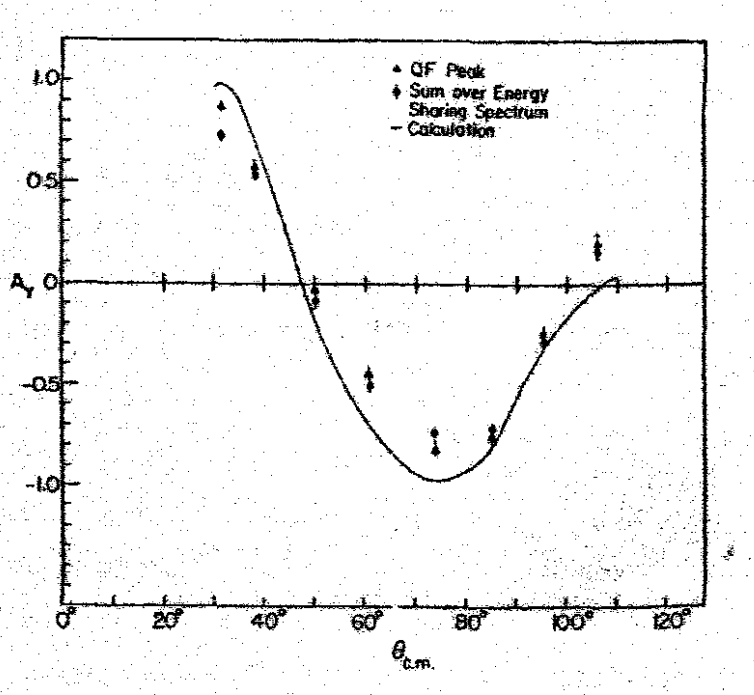

Figure 1.1: *$^9Be(p,p\alpha)^5He$ analyzing power data at the quasi-free peak (triangles) as a function of the two-body center of mass p-α scattering angle for an incident proton beam of 150 MeV [Wan85]. The circles represent A_y summed over the full energy sharing distribution. The curve represents free p-α data. This figure was taken from Wang et al. [Wan85].*

1.4 Inclusive (p, α) Measurements

In an inclusive α particle measurement the measured α particles originate from different nuclear reactions. Unlike in an exclusive measurement where a lot of possible reactions are excluded because of the design of the experimental setup, in an inclusive measurement

all possible α particle energies and different α reactions are included. An example of an exclusive measurement is where an experiment is set up to look at coincident protons and α particles when using an incident proton beam, whereby reactions such as e.g. $(p, \alpha d)$, $(p, 2\alpha)$ and $(p, \alpha t)$ are automatically excluded. In this measurement the experiment looks exclusively at those reactions that cause protons and α particles to emerge from the target at the same time.

Nevertheless inclusive $(\overrightarrow{p}, \alpha)$ measurements can be used to investigate α clustering. It is however important to measure the analyzing power and not cross section only because studies of the inclusive ^{58}Ni$(\overrightarrow{p}, \alpha)$ done by Bonetti *et al.* [Bon89] showed clearly that the cross sections alone are not sensitive to the reaction dynamics as are analyzing power distributions.

Analyzing power emission energy distributions for the inclusive $(\overrightarrow{p}, \alpha)$ reactions on ^{59}Co at an incident energy of 100 MeV were investigated by Cowley *et al.* [Cow02]. The focus was on the extent to which the first step direct knockout determines the emission of α particles. The DWIA (Distorted Wave Impulse Approximation) was used to evaluate the results from a simple α cluster knockout model. The results were compared with the $(p,^3$He) reaction on ^{59}Co at an incident energy of 100 MeV. It was concluded that a one step mechanism dominates the emission of α particles for small energy transfers. It was also found that the single step mechanism appears to persist to higher excitations of the residual system for the (p, α) reaction than was found for $(p,^3$He) case.

On the other hand Renshaw *et al.* [Ren91] found that the analyzing powers for mass fragments emitted in inclusive measurements of protons from ^{nat}Ag at 200 MeV are consistent with zero. This did not give evidence for a significant contribution from cluster knockout.

1.5 Aim of this Experiment

This research project Pr96a by [Nev04] investigated the analyzing power of the ^{40}Ca$(\vec{p},p\alpha)$ reaction at 100 MeV for different coplanar quasi-free angle pairs (i.e. angle pairs at which knockout of alpha particles at rest in the target nucleus is kinematically accessible). The region of interest is indicated in Fig. (1.2). The datapoints indicated represent free p-α elastic scattering data at 100 MeV [Nad83] as a function of the p-α center of mass scattering angle. The choice of ^{40}Ca as a target is based on Fig. (1) of Ref. [Car84], which suggests that for the heavier targets the probability of alpha cluster formation is at a maximum for target mass around 40.

The focus of this project is on some particular aspects of the data collection and analysis, namely the investigation of the inclusive ^{40}Ca$(\vec{p},\alpha)$ measurement. Inclusive ^{40}Ca$(\vec{p},\alpha)$ analyzing powers are calculated from the α singles data. α clustering is also investigated in this study, since analyzing power data from the measurement and knockout calculations can be used to comment on the existence of an α particle cluster inside the ^{40}Ca nucleus.

A very important aspect of the data analysis is to ensure that the quality of the data for each weekend is sufficient and that the results from the various datasets can be added together without comprising the quality of the final coincidence data. The determination of the inclusive ^{40}Ca$(\vec{p},\alpha)$ analyzing power for each data set is crucial to attain this goal, as the cross section for this measurement is much higher than the ^{40}Ca$(\vec{p},p\alpha)$ measurement cross section. This is because exclusive measurements are very selective about interactions and specific kinematics are involved, which result in lower statistics. In the experiment it was found that a few coincidence reactions ($\approx$300 coincidences per weekend) take place while the detectors detect thousands of particles per second. Therefore singles or inclusive $(\vec{p},\alpha)$ measurements are often used for exclusive measurement's data quality check. Since the cross section of inclusive measurements is much higher than that of the exclusive measurement, comparing datasets of different runs and scattering angles on a day-to-day basis is only practical with the inclusive data.

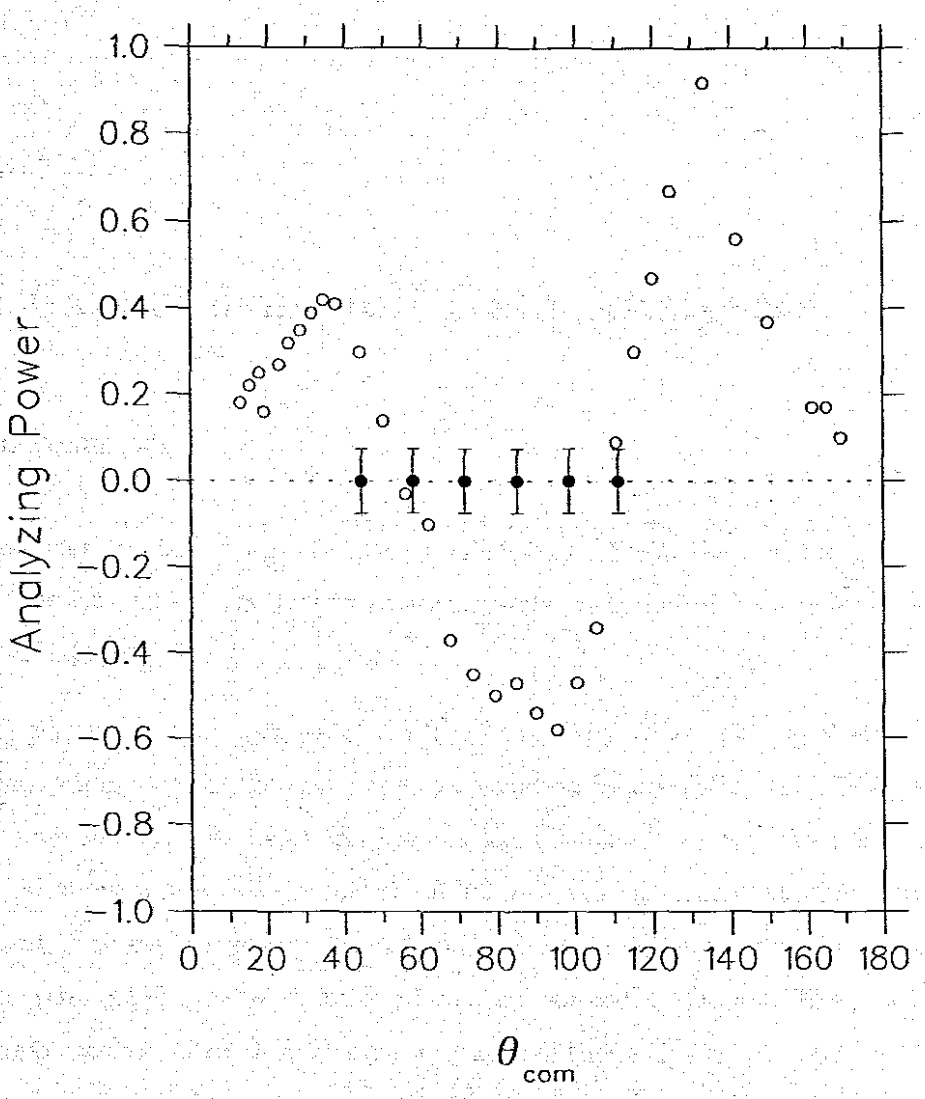

Figure 1.2: *The empty circles represent free p-α analyzing power data at 100 MeV from Ref. [Nad83], displayed as a function of the two-body center of mass p-α scattering angle. The filled circles represent the range of the center of mass angles that will be covered by this and subsequent studies of the $^{40}Ca(p,p\alpha)$ reaction. The error bars denote the expected statistical error of the measurement. The indicated A_y value of zero is of course of no significance, and must be experimentally determined. This figure is taken from Ref. [Nev04].*

Chapter 2

The Experiment and Data Analysis

2.1 Overview

The experiment PR96a was performed at iThemba LABS in the K600 magnetic spectrometer experimental area. Data was acquired over a period of five weekends between 23 July and 23 August 2004.

The $(\vec{p},p\alpha)$ reaction consists of a three body final state. This final state can be determined using momentum and energy conservation by measuring the kinetic energies and the angles of the outgoing particles at a known incident energy. Two detector systems, a silicon detector telescope and the K600 magnetic spectrometer, were used in this experiment. The nuclear interaction is spin dependent, and by polarizing the beam into two spin states one can get additional information out of the reaction. The proton beam was therefore polarized to allow the measurement of the analyzing power.

In this chapter the experimental set-up and analysis procedures are discussed. Information on the proton beam is given, followed by a description of the scattering chamber. The detectors and the targets that were used during the experiment and the electronics required for signal processing are described. Data acquisition and computer software for data handling are explained and the experimental procedure and the data analysis procedure are discussed. Lastly the error analysis is discussed.

2.2 The Proton Beam

iThemba LABS has two solid-pole injector cyclotrons, namely the SPC1 (Solid-Pole Cyclotron), which is used for the first stage acceleration of light-ions, and the SPC2, which is used for the first stage acceleration of the heavy ions and polarized proton beams. A polarized ion source is used to produce the polarized proton beam. The SSC (Separated Sector Cyclotron) with its four sector magnets is used to accelerate ions to the final energy. For this experiment the beam was steered from the SSC along the X, P1, P2 and S lines to the spectrometer vault. An overview of the facility is given in Fig. (2.1). This experiment used a 100 MeV polarized proton beam, thus SPC2 was used.

2.2.1 Polarized Proton Beam

Spin 1/2 particles can be described in terms of spin projection along the quantization axis. When the spin projections of particles in a beam of particles are all aligned, the beam is said to be fully polarized. The polarization degree of the beam refers to the fraction of the particles with the desired alignment. The proton beam was polarized perpendicular with respect to the scattering plane. The beam was automatically cycled between spin up and spin down orientations every 10 seconds.

Beam polarization is measured using scattering from targets with a known value for the analyzing power (A_y). At iThemba LABS it can be determined in either the low energy polarimeter between SPC2 and the SSC (K-line), or the high energy polarimeter in the P-line. To determine the beam polarization, a ^{4}He target was used at the K-line and a CH_2 target was used at the P-line. The P-line polarimeter is routinely used to determine beam polarization during the experiment, while the K-line is used to optimize the degree of polarization prior to the experimental runs. Polarization was determined by

$$p^{\uparrow} = \varepsilon^{\uparrow}/A_y \ , \tag{2.1}$$

Run-nr	$p^{\downarrow}$(%)	$p^{\uparrow}$ (%)
127-140	87.7	74.2
209-237	80.6	80.2
219-237	86.4	76.7
310-326	83.7	73.9
328-338	80.3	69.9
409-439	83.9	77.1

Table 2.1: *Spin-down and spin-up beam average polarization measurements for PR96a [Nev05]. Run-nr represents the run number to which the polarization values are applicable.*

where

$$\varepsilon^{\uparrow} = \frac{L^{\uparrow} - R^{\uparrow}}{L^{\uparrow} + R^{\uparrow}} , \tag{2.2}$$

and

$$p^{\downarrow} = \varepsilon^{\downarrow} / A_y , \tag{2.3}$$

where

$$\varepsilon^{\downarrow} = \frac{L^{\downarrow} - R^{\downarrow}}{L^{\downarrow} + R^{\downarrow}} . \tag{2.4}$$

where $L^{\downarrow(\uparrow)}$ and $R^{\downarrow(\uparrow)}$ represent the amount of the events registered in the left and right detector associated with the downward (upward) beam polarization respectively. Averaged polarization values for spin-up and spin-down are summarized in Table (2.1).

2.3 Scattering Chamber

A scattering chamber is an enclosed space where the reaction takes place. The K600 scattering chamber has a single rotatable table onto which a brass collimator and the Si-telescope is bolted. The target ladder can hold six targets and can be driven vertically so that any of the targets can be placed in front of the beam. It can also be rotated to different angles with respect to the beam.

In the side of the chamber there is one port which was used as a window to enable

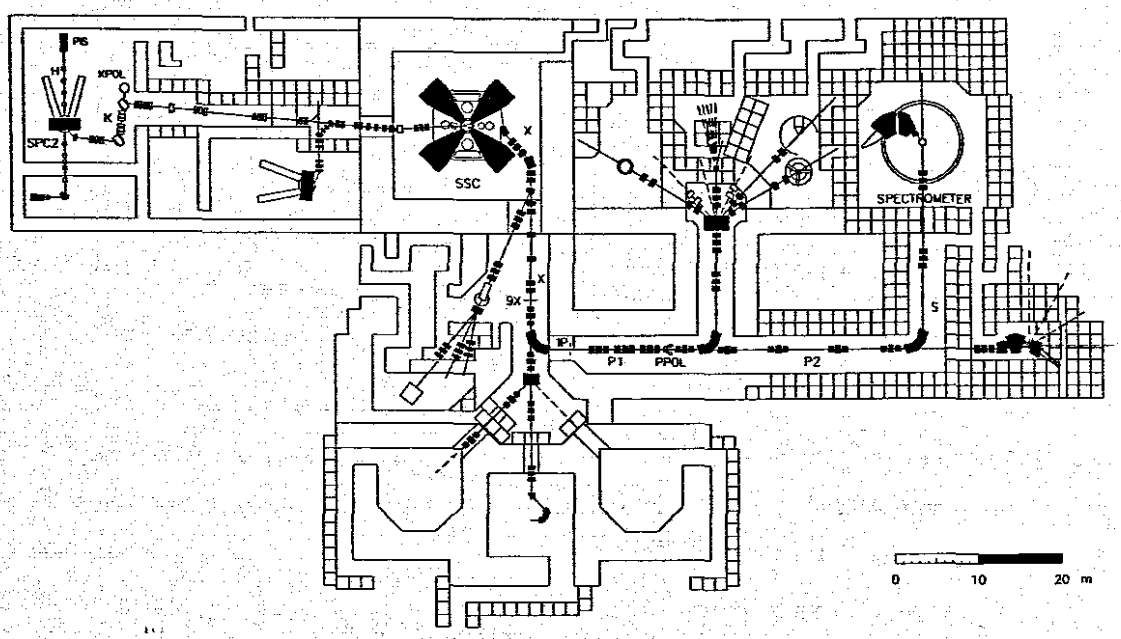

Figure 2.1: *Layout of the facilities at iThemba LABS.*

the camera to view the position of the target. This is required for the beam alignment procedure. The scattering chamber was kept at a very low pressure (10^{-5} mbar).

2.4 Detectors

Three silicon detectors of different thicknesses were used to make up the Si detector telescope, which was used to detect α particles. The protons were detected using the K600 magnetic spectrometer, which was on the opposite side of the beam from the Si detectors. Since this thesis only concerns the $(\vec{p}, \alpha)$ interaction the rest of the discussion will focus on the alpha particle detector.

The Si detectors used in this experiment are surface barrier detectors. These detectors rely on the junction formed between the n-type silicon semiconductor with gold. These materials have different Fermi levels, therefore a contact emf arises when the two are put together. A lowering of the band levels in the semiconductor is therefore caused. By applying a reverse bias, a depletion zone that extends entirely into the semiconductor is formed, and the entire volume is thus effective as a charged particle radiation detector.

2.4.1 Si-Telescope

As mentioned above, the Si detector telescope consisted of three detectors: the detector closest to the target, the so-called ΔE detector, was 94.8 μm thick. The middle detector, referred to as the E detector, was 2027 μm thick. The last detector, also called the veto detector, was 1022 μm thick. This is shown in Fig. (2.5). These detectors were in the vacuum environment of the scattering chamber.

The thickness of the first two Si detectors was chosen to allow the α particles to easily pass through the thin first detector and stop in the second, thicker detector. The ΔE detector was then used to measure the energy loss of the particle as it passes through, and the E detector was used for the measurement of the energy of a particle that comes to rest inside this detector. By combining the information of these two detectors particle identification can be achieved, as different types of charged particles have different ΔE-E characteristics. This can be seen in Fig. (2.7), which is a two dimensional plot of the pulse height information from the ΔE and the E-detectors. The relevant particles are indicated in the figure.

The veto detector was used for discarding particles that are not needed in the experiment, and in this case those particles are high energy protons. In this way, when the veto detector registers a signal, the data associated with that signal can be removed from the subsequent analysis. This is done because in this experiment we are only interested in detecting α's in the Si detector telescope, and not the protons.

A brass collimator was mounted in front of the silicon detector of the telescope. It was used to define the solid angle subtended by the detectors. The solid angle Ω of the silicon detector telescope was calculated as follows:

$$\text{Solid angle}(\Omega) = (\pi r^2)/d^2 \,, \tag{2.5}$$

where r is the radius of the collimator and d is the distance from the target to the back of the collimator. The ΔE-E detector telescope subtended a solid angle of 2.85 msr.

The collimator needs to be thick enough so that a 100 MeV proton from any other

angle cannot pass through. To determine the appropriate thickness of a collimator, energy loss calculations were done with the computer program called ELOSS. It uses the Bethe-Bloch approximation to calculate energy loss of a particle as it traverses matter. The parameters of interest are the type of incident particle and its incident energy, the type of target and density and the thickness of the target. The minimum required thickness of a collimator was determined to be 1.4 cm, the actual thickness of the collimator used in this experiment was 2.1 cm.

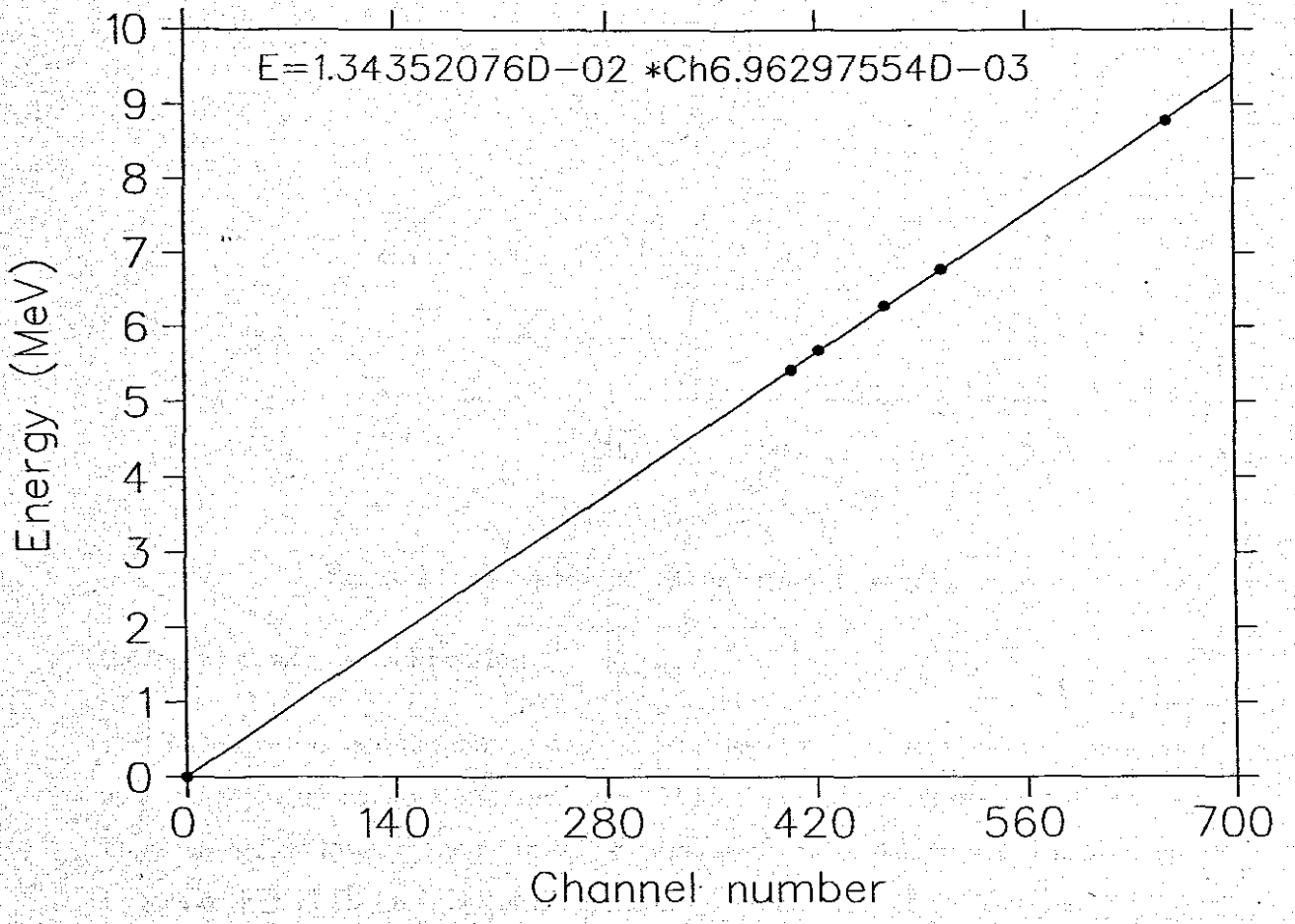

Figure 2.2: *Calibration spectrum for the ΔE detector.*

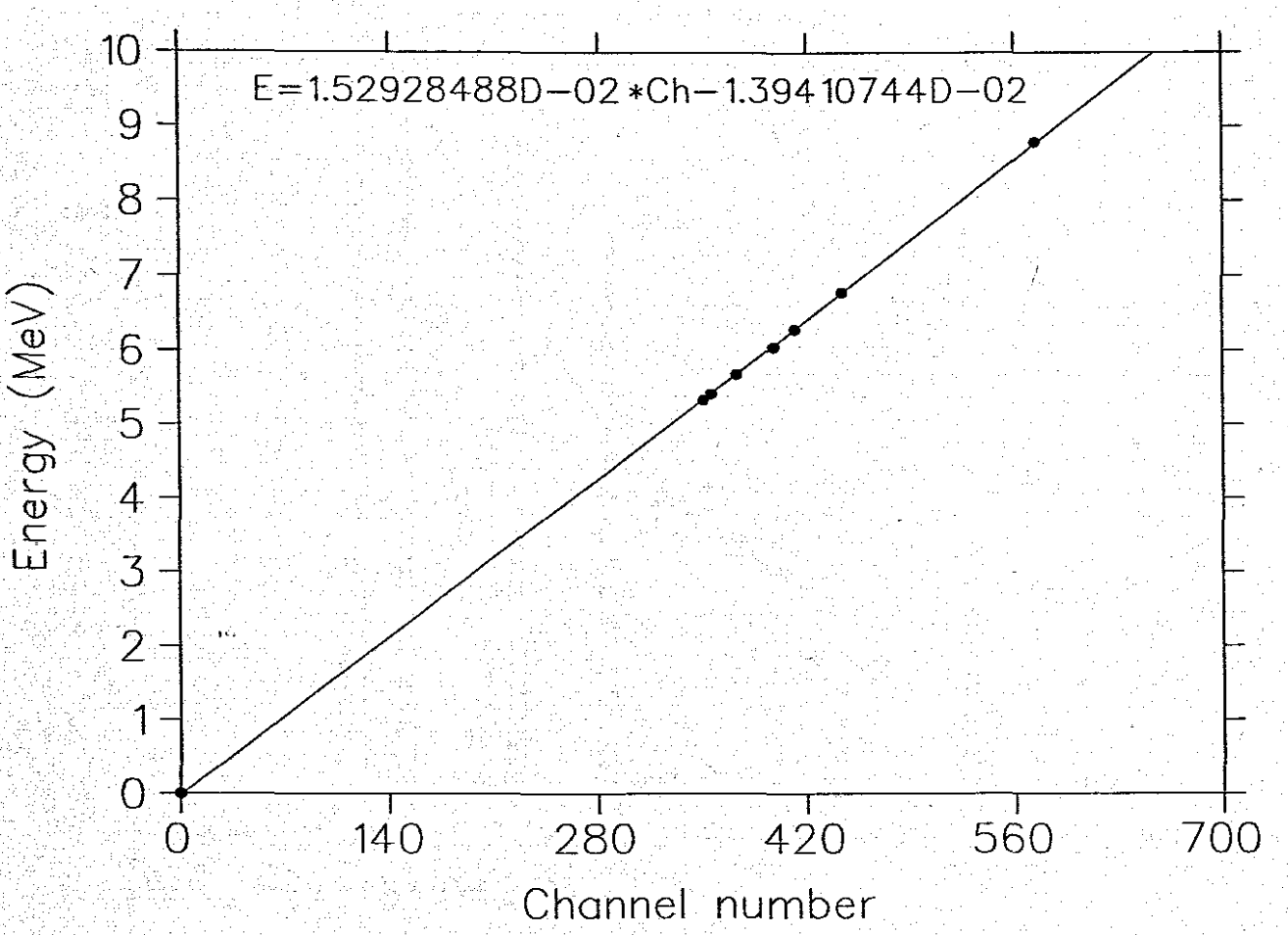

Figure 2.3: *Calibration spectrum for the E detector.*

2.4.2 Si-Detector Calibration

A ^{228}Th source was used to calibrate the E and ΔE detectors. The source emits α particles at energies ranging between 5.34 MeV and 8.78 MeV where the first two peaks from the lowest energy are from ^{228}Th and the other peaks are from the daughter nuclei. This can be seen on Fig. (2.4). Pulse height information was obtained for these detectors, and the peaks seen were easily identified from the known α energy spectrum. Using these different α energies and the channel numbers of the raw pulse height spectra obtained with the XSYS (Section 2.7 for more on XSYS) analysis software a linear fit was performed with a program called PHYSICA. The slopes and offsets were determined for the detectors, and

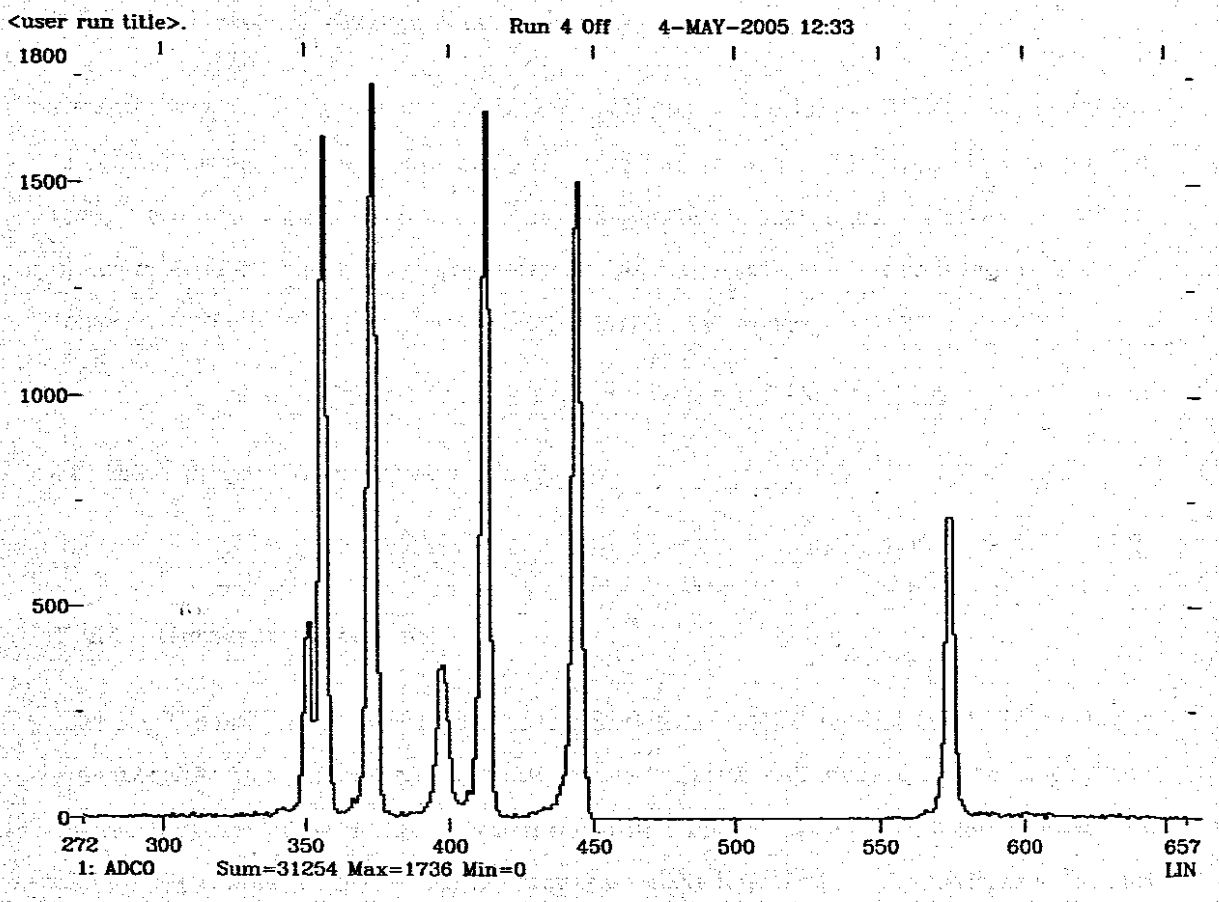

Figure 2.4: ^{228}Th *spectrum with the following energies from the lowest energies to the highest energies, 5.34054 MeV, 5.42333 MeV, 5.658856 MeV, 6.05098 MeV, 6.22829 MeV, 6.7785 MeV and 8.78437 MeV where the first two peaks from the left are from* ^{228}Th *and the others are daughter nuclei.*

they were as follows. For the E-detector

$$\mathrm{E(MeV)} = 1.529 \times 10^{-2} \times \text{channel no.} - 1.39 \times 10^{-2} \,. \tag{2.6}$$

For the ΔE detector:

$$\mathrm{E(MeV)} = 1.343 \times 10^{-2} \times \text{channel no.} + 6.96 \times 10^{-3} \,. \tag{2.7}$$

This is shown in Figs. (2.2) and (2.3) respectively.

2.4.3 Si-Detector Energy Resolution

Detector energy resolution was measured in terms of the full width at half maximum (FWHM) of the full energy peak of the ^{228}Th (8.78437 MeV peak). The better the energy resolution the better a detector will be able to distinguish between two peaks close in energy. The thicker the detector the better the resolution because it is not sensitive to electronic noise. For the ΔE detector the α energy resolution was

$$= \mathrm{m} \times \mathrm{FWHM} = 1.343 \times 10^{-2} \times 15 = 2.0145 \times 10^{-1}\ \mathrm{MeV}\ . \tag{2.8}$$

For the E detector α energy resolution was

$$= \mathrm{m} \times \mathrm{FWHM} = 1.544 \times 10^{-2} \times 4 = 6.1 \times 10^{-2}\ \mathrm{MeV}\ . \tag{2.9}$$

2.4.4 Detector Placement

The angle pairs for the positioning of the Si detector telescope and the K600 magnetic spectrometer were chosen so that the residual undetected nucleus in the coincidence measurement is left with zero or small recoil momentum. The calculation to determine the angles is done with a computer program called KINMAT. This program calculates two particle kinematics for particles that travel at relativistic speeds. KINMAT is used to approximate the three-particle system of knockout at zero recoil momentum by taking the Q-value of the knockout reaction into consideration. For the ^{40}Ca$(\vec{p},p\alpha)$ reaction the Q-value is -7.04 MeV and it is calculated as follows:

$$E = 931.5 \times (M_{Ca} - (M_{\alpha} + M_{Ar}) \tag{2.10}$$

where 931.5 is the energy mass equivalence of a proton and M_{Ca}, M_{α} and M_{Ar} respectively represent the mass of ^{40}Ca, an α particle and the residual ^{36}Ar nuclei. The Q-value is less than zero because the reaction has certain threshold energy, and some of the kinetic energy of the incident protons is required to emit the α particle.

Coincidence proton alpha energy spectra were measured at the angle pairs $(\theta_p, \theta_\alpha)$ = (59.1°;-51.5°), (70°;-45.5°) and (81°;-40.12°).

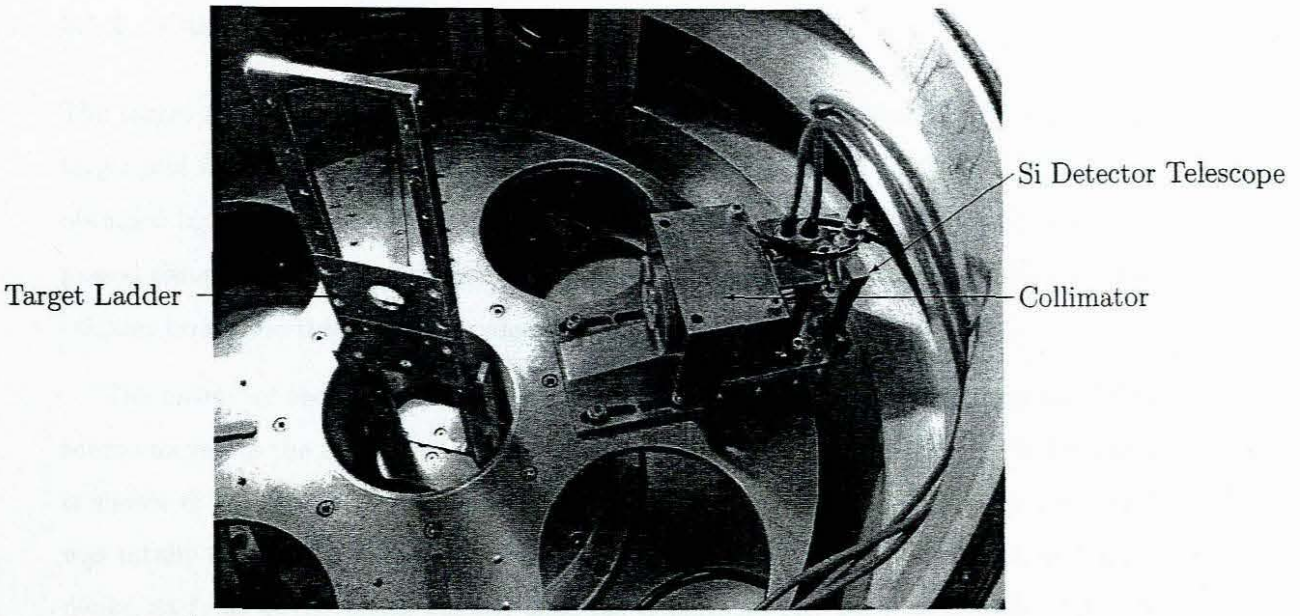

Figure 2.5: *The experimental setup of the Si detector telescope inside the scattering chamber. The target ladder, the brass collimator block as well as the three Si detectors can be seen in this picture.*

2.5 Targets

Two different targets with different thicknesses, a 2.38 mg·cm^{-2} thick ^{40}Ca target and a 2.65 mg·cm^{-2} thick ^{40}Ca target, were used in the experiment. Calcium targets should be handled with care and they must be kept in vacuum. In contact with air, calcium oxidizes very quickly. Two targets were used because we wanted to improve the target.

Other targets found on the target ladder include a ruby target, which was used for tuning a finely focused beam spot at the central position. An empty target frame was used to check the background or beam halo.

2.5.1 Calcium Target Thickness

The target thickness (in mass per unit area) can be roughly estimated by weighing the target and measuring its surface area. A more precise measure of the ^{40}Ca thickness was obtained by measuring the energy loss by alpha particles from the ^{228}Th source as they passed through the target. From the measured energy loss of the alpha particles in the calcium target the thickness was calculated.

The energy of the α particles was also measured when the particles from the ^{228}Th source moved to the detectors without passing through any target. The spectrum found is shown in Fig. (2.4). A spectrum found when the particles moved through the target was totally different from the one which was expected because this spectrum had many peaks, and one of the peaks showed that the α particles did not loose energy. Thus, it was concluded that the target has small holes. The target was also visually inspected and it was seen that it has small holes.

It is usually assumed that the thickness of a target is uniform and in an experiment the proton beam is focussed and steered to hit the target at the center. In view of the fact that there are small holes in the targets, consequently the thickness of a target is not uniform. This non-uniformity of the target results from the target manufacturing process. The number of measured particles depend amongst other things, on the target thickness. Thus because target thickness changes, the number of particles measured also changes. The hole problem caused us to use a second ^{40}Ca target because we wanted to improve the target by making it with fewer holes.

2.6 Electronics

iThemba LABS utilizes NIM (Nuclear Instrument Module) and CAMAC (Computer Automated Measurement and Control) fast electronic hardware to process the timing and energy signals from the detectors. The electronics diagram for both timing and energy signals is shown on Fig. (2.6).

2.6.1 Timing Signals

The signals from each of the three Si-detectors were processed by pre-amplifiers, where the signal strength was increased. The timing signals of the pre-amplifier were driven to the TFA (Timing Filter Amplifier), where they were amplified and shaped for further processing. The signals were then processed by the CFD (Constant Fraction Discriminator) unit. Here logic signals were generated at a constant fraction of the peak height of the input signal to produce an essentially walk-free timing signal. Signals from the CFD were further processed by a delay box. This box provided adjustable delays which allows a lengthening or shortening of the electrical paths in a circuit, since it had to be assured that the electrical paths along which two coincident signals travel to the coincidence unit are equal.

The signals were then processed by a logic unit which acts as an AND gate. This is where the coincidence of E and ΔE signals can be determined. A logic output signal is produced if E and ΔE signals are in coincidence and no signal is produced if the coincidence condition is false. All events where the veto detector saw a high energy proton and the events where a particle triggered only the E detector and not the ΔE detector were ignored. The pulses were finally transferred to the scalers, pattern register and event trigger CAMAC units. A schematic diagram of the electronics is given in Fig.(2.6).

2.6.2 Energy Signals

Energy signals represent one of the two types of signals which are generated in the preamplifiers. It gives accurate information about the amplitude of the signals and thus the energy of the particles.

The signals from the ΔE detector, E detector and veto detector were processed by different pre-amplifiers, where they were amplified and then processed by a spectroscopy amplifier where they were amplified and shaped to allow pulse height determination. They were further processed by delay amplifier and then by linear gate and stretcher (LGS),

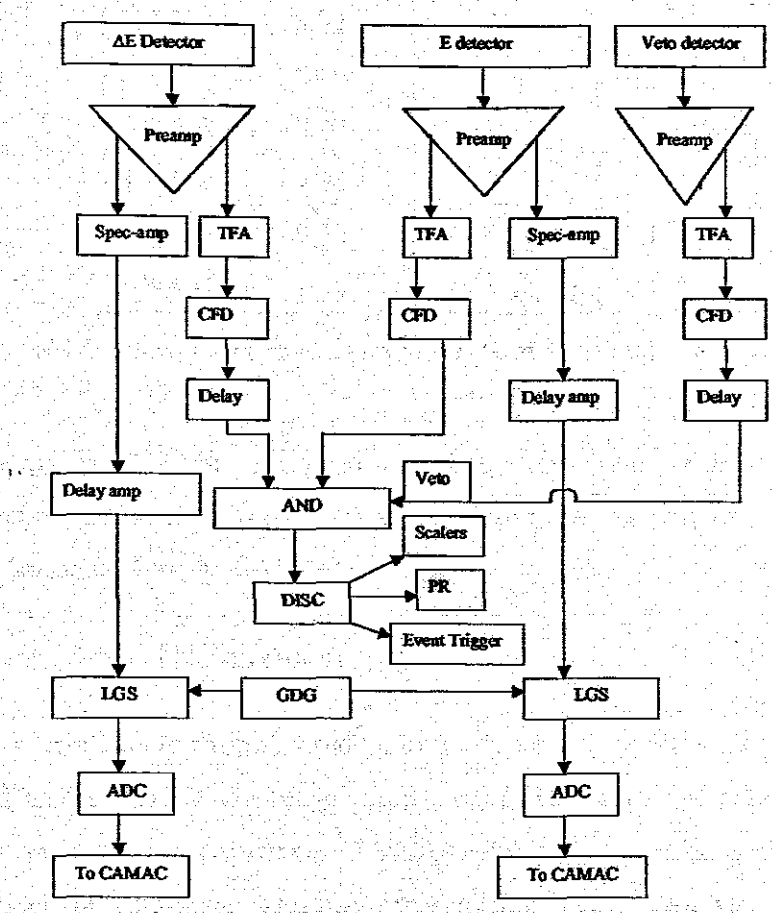

Figure 2.6: *NIM-electronics for timing signals and energy signals.*

where the linear gate functions as a pulse signal switch which allows linear signals at its input to pass through only if there is a another coincidence signal present, otherwise the signal is blocked. The stretcher is a pulse shaping module which prolongs the duration of

Run number	Computer dead time %	Electronic dead time %	Total time (hours)
127-134	5.34	7.82	8.18
209-214	6.56	8.70	9.43
219-237	3.42	7.40	19.93
310-326	4.58	8.12	21.01
328-337	2.82	8.28	16.08
409-438	3.19	6.61	45.55

Table 2.2: Weighted-averages of the computer dead time and the electronic dead time, and the total run time.

an analog signal at its peak value. The signals were then transferred to the analog to digital converter (ADC) where the analog signal amplitude was digitized. This information was then transferred to the CAMAC system.

2.6.3 Dead Time Measurement

The main corrections to the measured number of counts come from data acquisition dead times and inefficiencies in the trigger hardware. In the process of data handling by the data acquisition system, acceptance of additional data becomes impossible as a result of the busy state of the system. This process is called computer dead time. Computer dead time was measured using a pulser and two CAMAC scalers. One CAMAC scaler was inhibited by a computer busy signal and the other was uninhibited and they are referred to as pulser inhibited and pulser uninhibited respectively. Computer dead time can be calculated using the ratio between the pulser inhibited and the pulser uninhibited values.

Electronic dead time is caused when triggers are missed because the trigger hardware is busy when an event that should generate a trigger comes in. When a logic gate in the trigger is activated, the output signal stays high for a fixed time. If another event tries to activate the gate in that time, it is ignored. Electronic dead time was calculated using the ratio between the inhibited pulser scaler and the pulser peak counts observed in a

pulser spectrum.

Each of the pre-amplifiers of the detectors was provided with a pulser signal which is of the same origin as the pulser in the computer dead time. The rate of each pulser was proportional to the beam current. These pulser signals then move from the detector pre-amplifiers to the trigger hardware in the same manner as the signals representing measured particles does. By knowing how many pulser signals were sent to the detectors and by knowing how many made it through the trigger hardware, the electronic dead time of the trigger hardware can be determined. The scaler contains the information of how many pulsers were sent to the detectors. The pulser spectrum in the computer tells us how many pulser signals made it through the trigger hardware. Typical computer dead time values are between 2 % to 5% and typical electronic dead time value is ~10%. The weighted values of the computer dead time and the electronic dead time are listed on Table (2.2).

2.6.4 Current Integration

The beam current is determined at the beam stop. The total charge carried by the particles was determined by integration of the current using a current integrator.

2.7 Data Acquisition

CAMAC and NIM electronic hardware were used to process energy and timing signals from the E detector and ΔE detector. VME (Versa Module Eurocard) served as an interface between the VAX data acquisition computer and a CAMAC system. Data is handled by XSYS analysis software. XSYS analysis software runs two files, the COM and EVAL files. The COM and EVAL files used were ppa-manus-updw.com and ppa-manus-updw.evl respectively. The EVAL file uses data areas created in the COM file to sort and analyze the raw data from the buffers. The COM file defines all the data areas for all the histograms to be stored including the data areas for the gates.

2.8 Experimental Procedure

The electronics was put in place, the target ladder was placed inside the scattering chamber and the scattering chamber was pumped down to the required vacuum.

The 100 MeV proton beam was positioned at the center of the target. This was done using the scintillating properties of the ruby target. A video camera which was placed on one of the ports of the scattering chamber was used to view the ruby target.

Beam halo was minimized with the use of an empty target by tuning the proton beam until the count rate of the detectors reached a minimum. The beam was considered adequate if the count rate with the empty target is less 5 percent of the value obtained when there is a target.

The ^{40}Ca target was placed in the beam. Data acquisition was then started. Typical runs lasted for two hours or one hour, interrupted by P-line polarization measurement runs. Typical beam current was 30 nA.

2.9 Analysis Procedure

The data analysis was performed with a Vaxstation 4000 workstation using the XSYS analysis software. A Particle Identification (PID) spectrum was generated and then the α particles were selected using the ΔE-E technique. The Mass Function was also generated and the gate was set around the α particle loci. The pulse height information for the α particles was extracted and calibrated for all the various datasets of the different weekends. These counts were then converted into the analyzing power.

2.9.1 Si-Telescope Particle Identification

Particle identification was achieved by combining the information from the E detector and ΔE detector. Different types of charged particles have different ΔE-E characteristics and different loci as shown on Fig. (2.7). According to what is seen on the figure, protons seem to loose less energy in the ΔE detector than alpha particles of the same kinetic

energy. This is because according to the Bethe-Bloch approximation of energy loss of a particle as it traverses matter, energy loss is proportional to the atomic number of the particle and inversely proportional to its speed

$$\Delta E \propto Z^2/\beta^2 \tag{2.11}$$

where

$$\beta = (v/c). \tag{2.12}$$

Consider the fact that for a proton Z is 1 while Z of an alpha particle is 2 and that β of a proton is greater than that of an α particle with the same kinetic energy. It is obvious that the heavier alpha particle undergoes a much greater energy loss than the proton.

The mass function was used to improve the separation between different particles so that we could clearly distinguish between α particles and ^{3}He. The mass function was calculated as follows

$$\mathrm{MF} = [(E_{\Delta E} + E_E)^c - E_E^c] \times d\,, \tag{2.13}$$

where $E_{\Delta E}$ is the energy of ΔE detector, E_E is the energy of E detector, and c and d are constants. The separation was improved by changing c and d until different loci were clearly seen. The values for c and d which gave a good separation were found to be 1.7 and 4.0 respectively. Alpha particles were selected by setting a gate around the appropriate locus on the mass function. The gate was put on the mass function and not on the PID because the mass function is a straight line and there is a clear separation between different particle loci while the PID shape is complicated and the particles are not clearly separated. This is shown on Fig. (2.8).

2.9.2 Analyzing Power Calculation

The two bottom spectra shown in Fig. 2.9 are based on raw, non calibrated data where there is a spectrum from ΔE detector and E detector on the left and right respectively. The data is a combined count of protons, α particles and other particles. α particles were then selected on both spectra. These two spectra were calibrated and added together and the end result was a calibrated energy spectrum (the spectrum on top) which has α

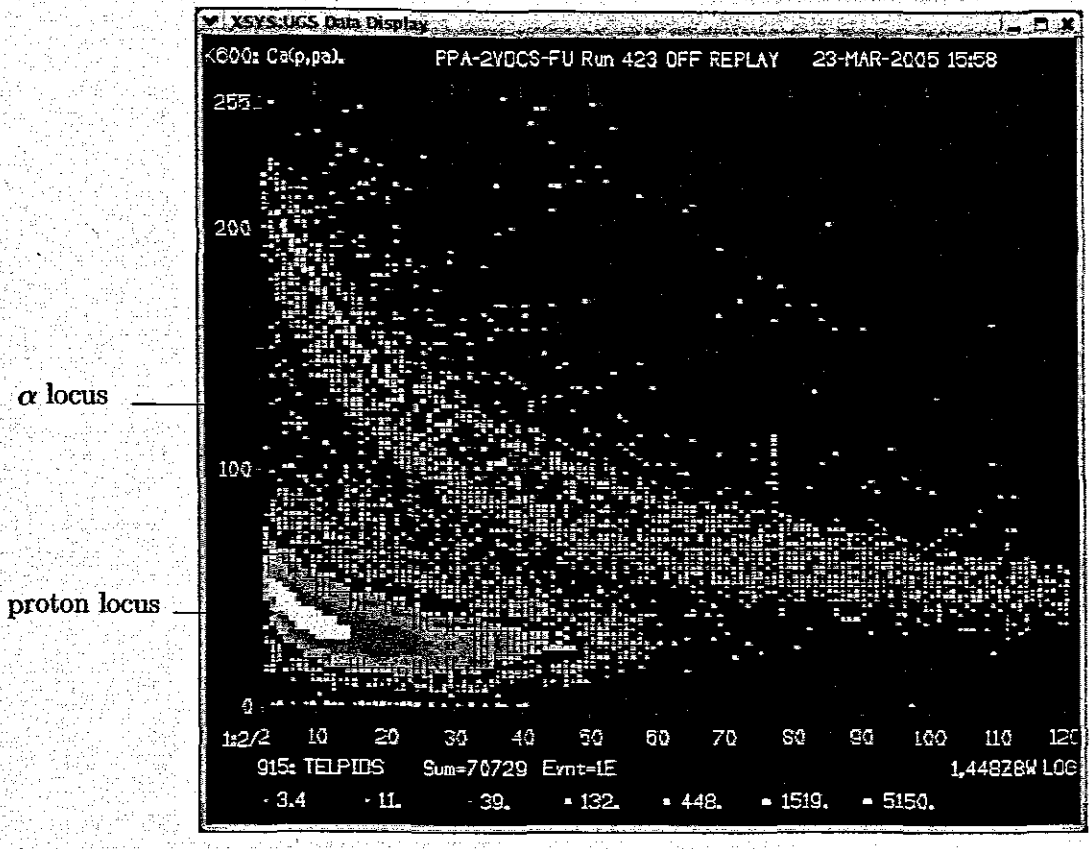

Figure 2.7: *A typical two dimensional plot of the pulse height information from the ΔE Si detector on the y axis versus the pulse height information from the E Si detector on the x-axis. The α locus is on top and the proton locus is at the bottom.*

particles only. The reason there is a space from zero to 390 is because the low energy particles did not trigger the second detector (E detector) because they stopped on the first detector (ΔE detector), so they were not included on the data. The spectrum was divided into chunks of 2 MeV bins.

The following formula was used to calculate the analyzing power

$$A_y = \frac{C^{\uparrow} - C^{\downarrow}}{C^{\uparrow}p^{\downarrow} + C^{\downarrow}p^{\uparrow}}, \tag{2.14}$$

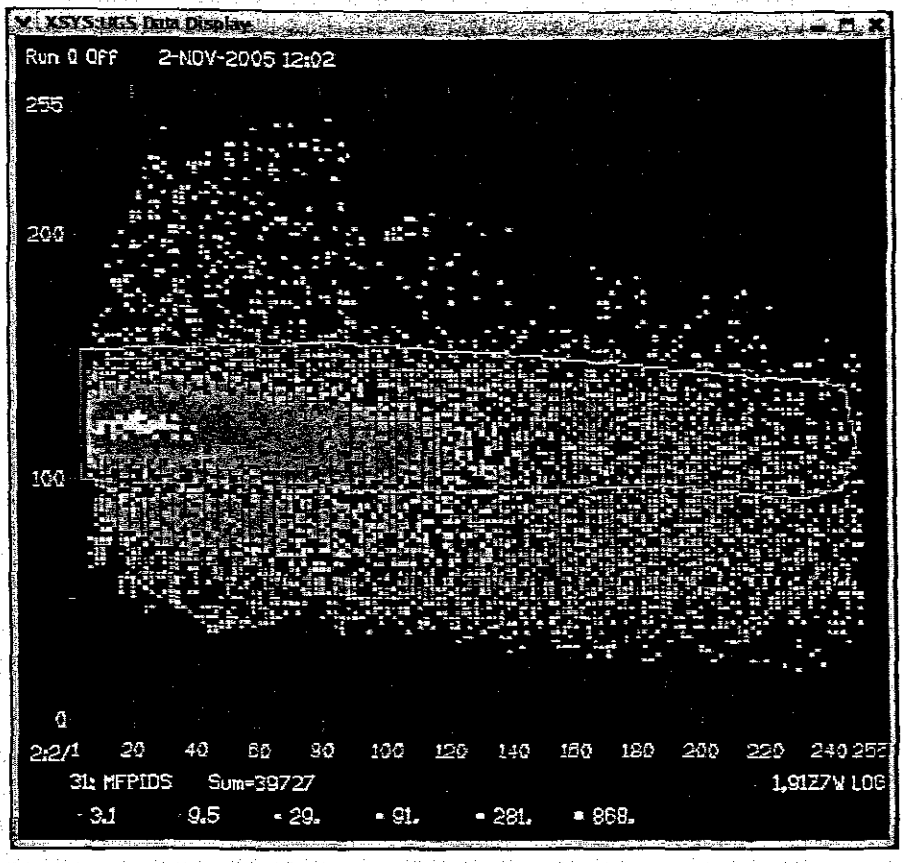

Figure 2.8: *Gated Mass Function. Mass function on the y axis and energy on the x axis. The gate is set around the α particles locus and there is a ^{3}He locus at the bottom.*

where $C^{\uparrow}(^{\downarrow})$ represents the total number of events per energy bin for the proton beam polarized in the upwards (downwards) direction, and $p^{\uparrow}(p^{\downarrow})$ represents the degree of polarization for the upwards (downwards) polarized beam.

Different measurements with different errors were combined using a weighted mean method [Leo87]. The weighted mean was calculated using the equation below

$$\mu = \frac{\sum_i \frac{x_i}{\sigma_i^2}}{\sum_i \frac{1}{\sigma_i^2}}, \tag{2.15}$$

where μ is the weighted mean, x_i is the analyzing power and σ_i is the statistical error. The error on the weighted mean $\sigma(\mu)$ is given by

$$\sigma(\mu) = \frac{1}{\sum_i \frac{1}{\sigma_i^2}}. \tag{2.16}$$

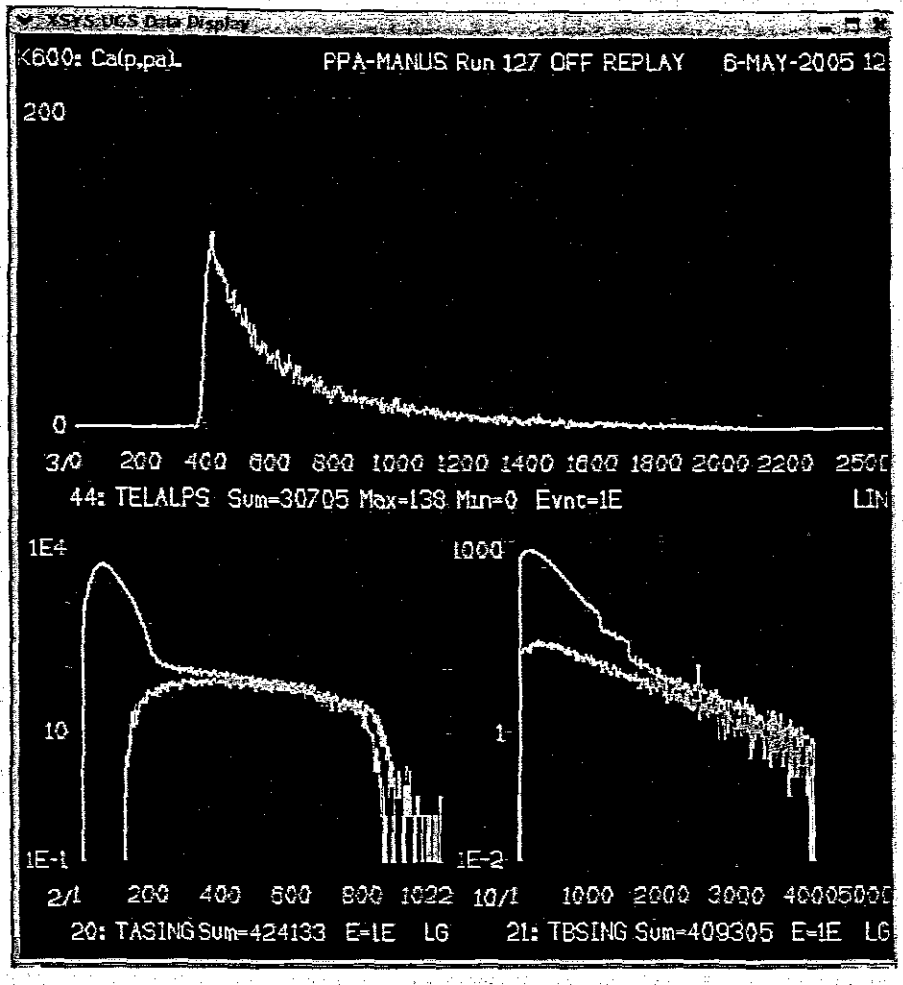

Figure 2.9: *Raw and calibrated spectrums. The two spectrums at the bottom are raw spectrums from ΔE (spectrum on the left) and E detector (spectrum on the right). On both spectrums the top curve consists of both protons and α particles and the bottom curve consists of α particles. The spectrum on the top is the calibrated spectrum.*

This was done because of the fact that some measurements are more precise than others and should therefore be given more importance. This was done by weighing these measurements in proportion to their errors.

The analyzing power calculations using Eq. (2.14) , Eq. (2.15) and Eq. (2.16) were done with computer software called PLOTDATA using PLOTDATA (pcm) files namely ap-wm.pcm and ap-comb.pcm, which were plotted in PLOTDATA.

2.10 Error Analysis

2.10.1 Systematic Errors

Systematic errors are uncertainties in the bias of the data. These errors mean that all measurements in a set of data taken with the same instrument are shifted in the same direction by the same amount. In this case these are the errors from the uncertainty in the solid angle, target thickness, energy calibration, degree of polarization and gates on the particle identification spectrum.

The analyzing power is defined in terms of ratios of spin-up and spin-down cross-sections Eq.(2.14), therefore systematic errors do not contribute in the determination of the analyzing power. This is because these variables (solid angle, target thickness) cancel. However, an uncertainty in the determination of the analyzing power occurs because of the uncertainty in the degree of polarization of the incident beam.

Solid Angle

The uncertainty of the solid angle is due to the uncertainties in the distance between the target center and the collimator and the radius of the collimator. The uncertainty in the hole radius of a collimator is ~ 0.1 mm and the distance between the target center and the collimator is ~ 0.01 mm. The uncertainty of the solid angle is $\sim 5\%$.

Si-Telescope Particle Identification

There is a possibility that some α particles might fall outside the gate which causes an uncertainty. This uncertainty is however small because the gate was carefully set and the alpha particles loci were separated from those of other possible particles.

Target Thickness

The uncertainty in the thickness is big, but it does not contribute on the analyzing power results because the analyzing power is not dependent on the target thickness.

Energy Calibration

The uncertainty from the energy calibration does not have an effect on the analyzing power values, but only on the position of the datapoints.

Polarization

The uncertainty in the degree of polarization has an impact on the analyzing power results. This can be estimated from the equation [Car99]

$$\delta A_y = A_y \frac{\Delta p}{p} \,. \tag{2.17}$$

The uncertainty of the polarization Δp (up or down) is ~ 0.02 %.

2.10.2 Statistical Errors

In the results to be presented in the next chapter, the error bars on the data points represent the statistical errors. These are errors arising from the measurement of inherently random processes. They are most easily seen in measurements of statistical processes such as radioactive decay and proton-proton scattering. The statistical error in a counting experiment is the square root of the number of counts. The statistical error for the analyzing power was calculated by [Nev01]:

$$\delta A_y = \left[\frac{\left(C^{\uparrow} + C^{\downarrow}\right)}{\left(C^{\uparrow}p^{\downarrow} + C^{\downarrow}p^{\uparrow}\right)^2} + \frac{\left(C^{\uparrow} - C^{\downarrow}\right)^2}{\left(C^{\uparrow}p^{\downarrow} + C^{\downarrow}p^{\uparrow}\right)^4} \cdot \left(C^{\uparrow}p^{\downarrow 2} + C^{\downarrow}p^{\uparrow 2}\right) \right]^{\frac{1}{2}} \,. \tag{2.18}$$

Chapter 3

Theoretical background

3.1 Introduction

The Distorted Wave Impulse Approximation (DWIA) serves as a theoretical model to describe quasifree knockout reactions at medium energies [Nev01]. Here the $(\overrightarrow{p},p\alpha)$ knockout reaction is divided into three parts, i.e. an incident projectile that interacts with the nucleus, a nucleon-α interaction which results in the incident proton being scattered and an alpha particle being knocked out, and the last one is the outgoing particles' wavefunctions which are distorted by the residual nucleus.

The introduction to the theory can be found in the thesis of Neveling [Nev01] and in the review articles by Jacob and Maris [Jac66] and Kitching *et al.* [Kit85]. Nadasen *et al.* [Nad89] did measurements of the $(p,p\alpha)$ reaction on ^{9}Be at 200 MeV and analyzed the data in terms of the DWIA. The results confirm that the DWIA provides a good description of the ^{9}Be$(p,p\alpha)$ reaction at 200 MeV.

3.2 The DWIA

In the DWIA theory the triple differential cross section for the knockout reaction A$(\overrightarrow{p},p\alpha)$B, where the bound cluster has a total angular momentum J and an orbital angular momentum L is expressed as

$$\frac{d^3\sigma}{d\Omega_p d\Omega_\alpha dE_\alpha} = F_K S_{LJ} \frac{d\sigma}{d\Omega} \mid_{p-\alpha} \sum_{\Lambda} \mid T_{BA}^{\alpha L\Lambda} \mid^2 , \tag{3.1}$$

where F_K is a kinematic term made up of energy, momentum and angles terms of the initial and final particles in the knockout reaction, and

$$\frac{d\sigma}{d\Omega} \mid_{p-\alpha} , \tag{3.2}$$

is the two-body $p-\alpha$ cross section that represents the two-body interaction between the projectile and the bound α. S_{LJ} is a cluster spectroscopic factor that defines the probability of cluster existence. Eq. (3.1) represents a factorized form of DWIA where $\frac{d\sigma}{d\Omega}\mid_{p-\alpha}$ is factored out. A further approximation was made by using experimental $p-\alpha$ cross sections for Eq. (3.2) instead of two-body values. The term

$$\sum_{\Lambda} \mid T_{BA}^{\alpha L\Lambda} \mid^2 \tag{3.3}$$

is referred to as the distorted momentum distribution, it contains distorted wavefunctions and the bound state wavefunction of the α particle. The quantity $T_{BA}^{\alpha L\Lambda}$ is given by

$$T_{BA}^{\alpha L\Lambda} = \frac{1}{(2L+1)^{1/2}} \int \chi_{\alpha}^{(-)*}(r)\chi_{p}^{(-)*}(r)\chi_{p_0}^{(+)}(\gamma r) \times \phi_{L\Lambda}^{\alpha}(r)dr \ , \tag{3.4}$$

where $\chi_{\alpha}^{(-)*}(r), \chi_{p}^{(-)*}(r), \chi_{p_0}^{(+)}(\gamma r)$ are distorted waves for the incoming and the outgoing particles, γ is the ratio of the mass number of Ar to that of Ca and $\phi_{L\Lambda}^{\alpha}(r)$ is the bound state wavefunction of the α cluster in the target nucleus. α is the bound α particle, L is the orbital angular momentum of a bound α, Λ is the projection quantum number of L, B is the residual nucleus and A is the target nucleus.

In the optical model [Kra87] the scattering interaction is represented in terms of a complex potential U(r)

$$U(r) = V(r) + iW(r) \tag{3.5}$$

where V(r) is the real part which is responsible for the elastic scattering. In other words it describes the real interaction between the incident projectile and the target. W(r) is the imaginary part which is responsible for the absorption. The bound α cluster wavefunction was approximated by an eigenfunction of a Wood-Saxon potential well with an eigenvalue that is the same as the separation energy of the α particle from the target nucleus. The principal quantum number of the cluster is found from the conservation of oscillator shell model quanta.

Sub-channel	E_{lab} (MeV)	V (MeV)	r_0 (fm)	a_0 (fm)	W (MeV)	r'_0 (fm)	a'_0 (fm)	r_{0_c} (fm)
p+^{40}Ca	101.5	23.64	1.21	0.77	6.66	1.46	0.483	1.25
p'+^{36}Ar	65.0	35.65	1.21	0.77	0	0	0	1.25
α+^{36}Ar	29.5	151.01	1.26	0.767	14.24	1.69	0.519	1.30

Table 3.1: *Optical model parameters for ^{40}Ca. Note that entrance channel (p + A) potential depths have been scaled by $m_B/\, m_A$ [Car84].*

3.3 Inclusive Calculations

The analyzing power for the ^{40}Ca($\vec{p}$,α) reaction in terms of α cluster knockout is expressed as

$$A_y = \frac{\int A_{p-\alpha} \frac{d^3\sigma}{d\Omega_p d\Omega_\alpha dE_\alpha} d\Omega_p}{\int \frac{d^3\sigma}{d\Omega_p d\Omega_\alpha dE_\alpha} d\Omega_p}, \tag{3.6}$$

where

$$\frac{d^3\sigma}{d\Omega_p d\Omega_\alpha dE_\alpha} \tag{3.7}$$

is the cross section for the quasi-free knockout reaction ^{40}Ca($\vec{p}$,$p\alpha$)^{36}Ar and $A_{p-\alpha}$ is the analyzing power for the elastic scattering of an incident proton from the α cluster. The two-body analyzing power is approximated by the experimental values for (p,^{4}He) elastic scattering, and the integration is performed over the unobserved proton coordinates, represented by Ω_p.

The wavefunction of a quasi-free scattered proton is calculated with only a real optical potential in order to take into consideration the fact that the proton from the knockout process is not observed in the inclusive ($\vec{p}$,α) reaction. In other words the protons which were absorbed and those which escaped from the knockout process without undergoing any inelastic interaction with the recoiling nucleus are included in the calculation for the wavefunction of the quasi-free scattered secondary proton. Table 3.1 gives the optical model parameters for ^{40}Ca.

The central optical potential to generate the distorted waves is given by:

$$-U(r)_{central} = \frac{V}{1+e^{x}} + \frac{iW}{1+e^{x'}} + \frac{4iW_d.e^{x'}}{(1+e^{x'})^2} - U_{coul}(r)\ , \tag{3.8}$$

where

$$x = \frac{r - r_0.A^{1/3}}{a}\ , \tag{3.9}$$

and

$$x' = \frac{r - r'_0.A^{1/3}}{a'}\ . \tag{3.10}$$

The parameters used in Eq. (3.8), V is the strength of the real part of the central potential, W is the strength of the imaginary part of the central potential, W_d is the strength of the surface absorptive part of the potential. U_{coul}(r) is the Coulomb potential due to a sphere of radius $R_{coul} = 1.25$ fm.$A^{1/3}$, r_0 is a parameter for the radius of the real part of the central potential, r'_0 is a parameter for the radius of the imaginary part of the central potential, a is the real central diffuseness parameter, a' is the imaginary central diffuseness parameter and A is the atomic mass of the recoil nucleus.

3.3.1 THREEDEE calculations

The code THREEDEE is used for the calculations of knockout cross sections defined in Eq. (3.1). These calculations are carried out for each angle and energy of the knocked out α particle, as a function of the in-plane as well as the out-of-plane angles of the scattered proton. In order to calculate knockout cross sections three quantities must be generated, and they are the two-body scattering amplitude, the bound state wave function, and the distorted wave functions for the incoming and the outgoing particles. These calculations are done by firstly creating input files and then code THREEDEE is run using these input files. By running THREEDEE we get a file with the ^{40}Ca$(\overrightarrow{p}, p\alpha)$ cross section results.

Inclusive ^{40}Ca$(\overrightarrow{p}, \alpha)$ analyzing power calculations are performed with software called PHYSICA, where specific programs can be created. In order to get the corresponding two-body analyzing power, two-body LAB energy for final energy prescription which is the relative energy of the $p-\alpha$ system in the final state of the knockout reaction, and the center-of-mass two-body scattering angle are needed. These two variables were read from

an LST file (copap-ab-cd.lst where *ab* represents an angle and *cd* represents the kinetic energy of a knocked out α particle). After deciding on the two variables mentioned above the corresponding analyzing power was looked up in a data file. However, (p,^{4}He) elastic scattering data at 100 MeV - Q-value ($\approx$ 92.96 MeV) is not available therefore, interpolation between two known energies (85 MeV and 100 MeV) was performed. The free (p,^{4}He) elastic scattering analyzing power was multiplied by the ^{40}Ca$(\vec{p}, p\alpha)$ cross section as calculated by THREEDEE and lastly the analyzing power for ^{40}Ca$(\vec{p}, \alpha)$ measurement was calculated by integrating over the proton solid angle as shown in Eq. (3.6).

Chapter 4

Results

The results of the singles measurements done at 100 MeV as well as the theoretical calculations are presented in this chapter. Theoretical calculations were performed with the computer program THREEDEE.

4.1 Analyzing Power

The plots of the analyzing power versus α energy are shown in the figures (4.1) to (4.11). Firstly the datapoints for each weekend are plotted. Weekend 2 consists of one data set which was taken at 51.5°. Weekend 3 consists of two datasets that were taken at two different angles (51.5° and 45.45°). Weekend 4 also consists of two different datasets which were taken at two different angles (45.45° and 40.12°). Weekend 5 consists of one data set which was taken at θ_{Si}=40.12°. The different datapoints are shown in Figs. (4.1) and (4.2) for θ_{Si}=51.5°, Figs. (4.3) and (4.4) for θ_{Si}=45.45°, and Figs. (4.5) and (4.6) for θ_{Si}=40.12°. In all the above mentioned figures there are zero analyzing powers at low α energies and small negative analyzing powers at high α energies. The zero analyzing powers are caused by the polarization loss in the proton when it undergoes multiple scattering. This is due to multistep process. There are multistep reactions even at high α energies. α particles have different energies depending on the number of proton scattering steps before the formation of an α particle or the knockout of an α particle. There are non zero analyzing powers at high α energies because there are fewer steps that take place when the proton scatters before the formation of an α particle or when the α particle is knocked out. Fig. (4.7) shows two datasets which were taken at the same angle in four different weekends (from weekend 2 to weekend 5). In this figure three different angles are shown and for each angle there are two datasets. In Fig. (4.8) weighted mean results

of all the runs which were taken in different angles are shown. The weighted mean was calculated using Eq. 2.15. This was done with a PLOTDATA file called ap-allwm.pcm. Comparing $^{40}Ca(p,\alpha)$ results Fig. (4.8) with those of the $^{59}Co(p,\alpha)$ (Fig. 4.9) one can see that $^{40}Ca(\vec{p},\alpha)$ results at 51.5° are approximately the same as $^{59}Co(p,\alpha)$ results at 30°. Analyzing power distributions for $^{59}Co(p,\alpha)$ at 50° are above zero, $^{40}Ca(\vec{p},\alpha)$ at 51.5° are below zero. $^{40}Ca(\vec{p},\alpha)$ data only go to 60 MeV and not 90 MeV as for $^{59}Co(p,\alpha)$.

Fig. (4.10) shows the results of (p,^{3}He) (the spectrum at the bottom) where there are datasets for weekend 2 and weekend 3 plotted together and the results of ^{3}He and ^{4}He (the spectrum on top) plotted together, where the ^{3}He results are represented by triangles and the ^{4}He results are represented by circles. The ^{3}He analyzing power distribution is above zero for low α energies and below zero for high α energies except for the two datapoints that are at zero. This results give evidence that there is ^{3}He which was formed during the reaction. For ^{3}He and ^{4}He plotted together, the analyzing power distribution is above zero at low α energies, below zero at high α energies and zero analyzing powers are also there. These results are in good agreement with each other and they are consistent within the statistical error.

4.2 DWIA Results

In Fig.(4.11) the theoretical analyzing power is compared with the experimental data. Data was taken at three different angles. The solid line represents the theoretical predictions. In this figure two datasets plot as a function of energy and taken at the same angle are plotted together for all the three angles (40.12°, 45.45°, 51.5°). These datasets agree fairly well with each other and they are consistent within the statistical error. The theoretical predictions at the same angle are also plotted. The theoretical analyzing power at 51.5° is positive and non zero while the experimental data at the same angle has zero analyzing power at low α energies and analyzing powers below zero at high α energies. The theoretical analyzing power at 41.2° is positive while the experimental data has zero analyzing power and negative analyzing power. In other words the theoretical predictions

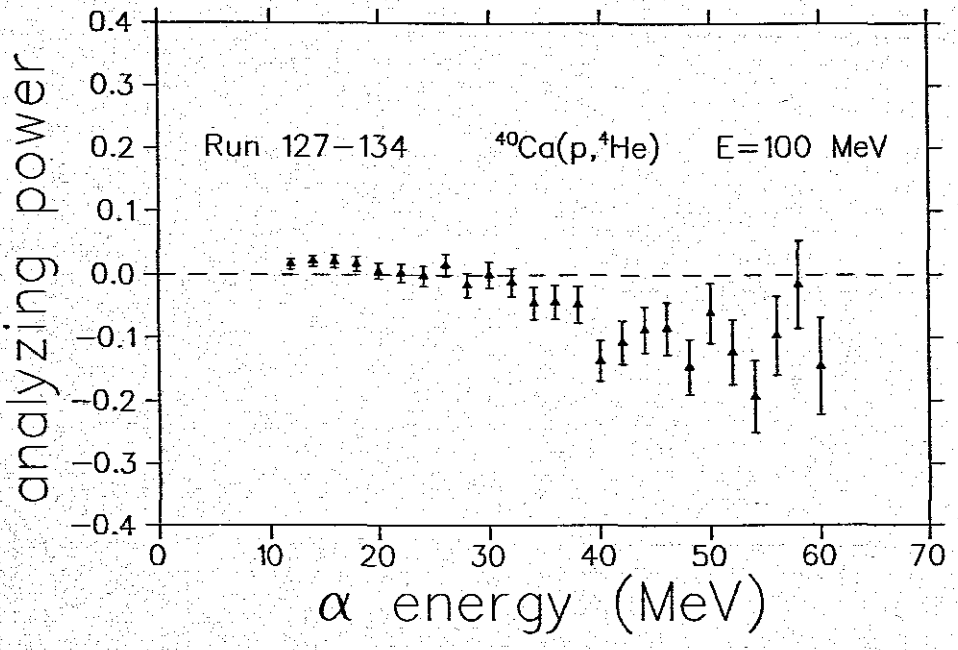

Figure 4.1: *Analyzing power results for weekend 2 taken at 51.5°. The error bars denote the statistical error of the measurement.*

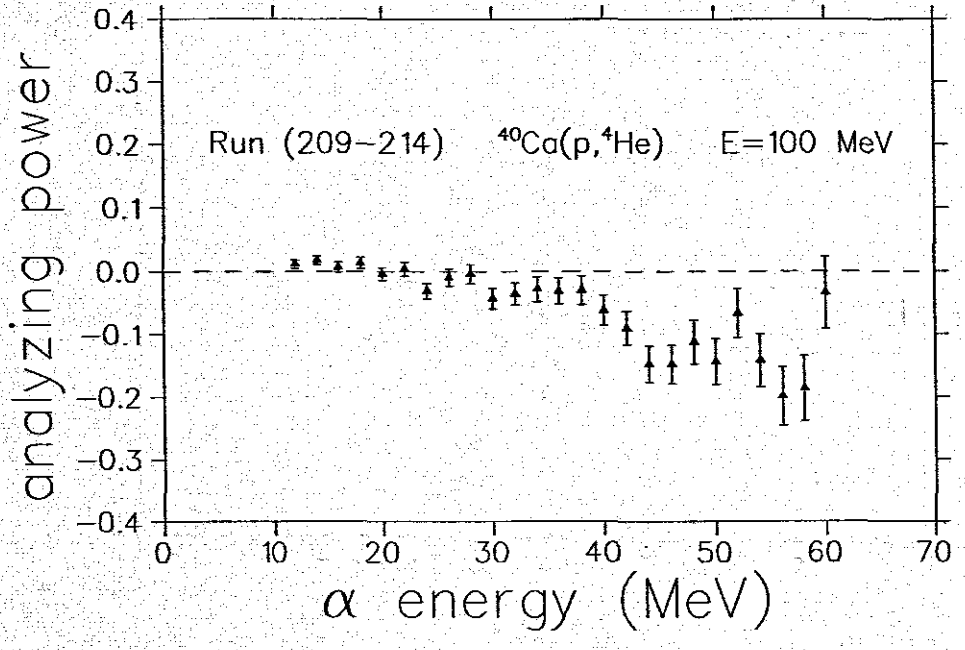

Figure 4.2: *Analyzing power results for weekend 3 taken at 51.5°. The error bars denote the statistical error of the measurement.*

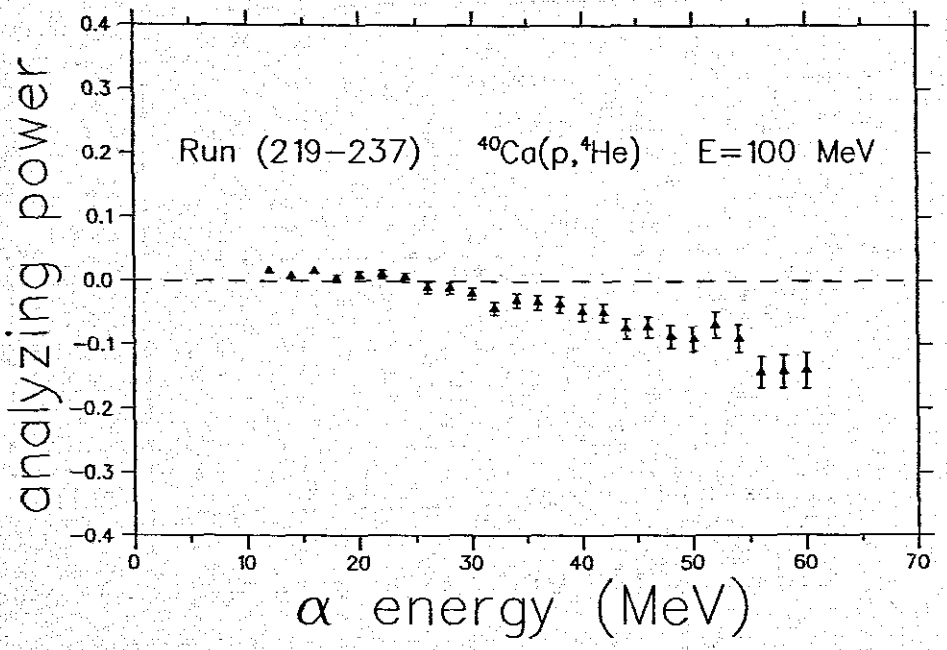

Figure 4.3: *Analyzing power results for weekend 3 taken at 45.45°. The error bars denote the statistical error of the measurement.*

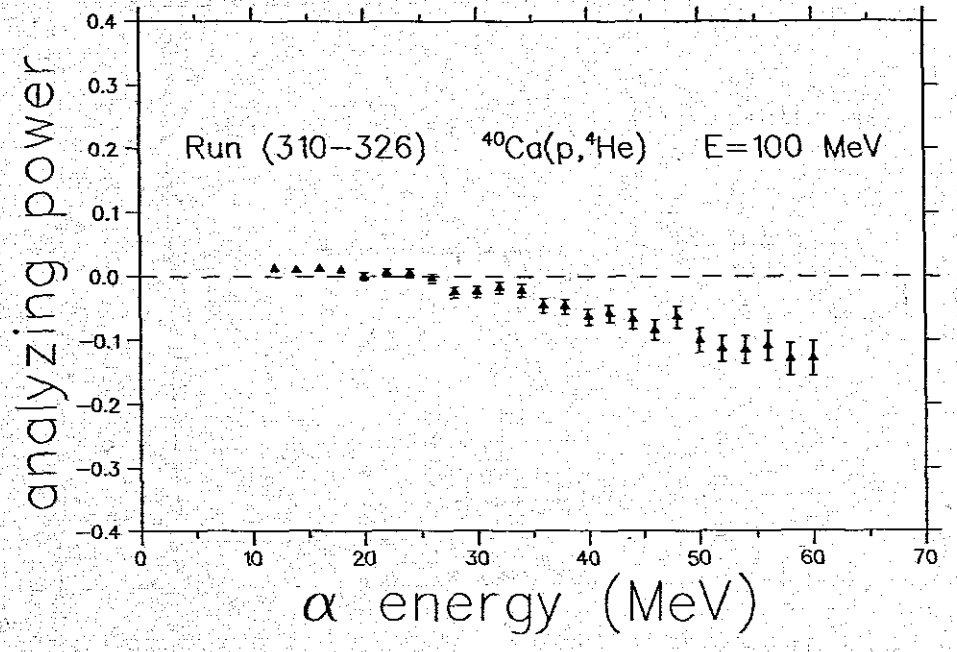

Figure 4.4: *Analyzing power results for weekend 4 taken at 45.45°. The error bars denote the statistical error of the measurement.*

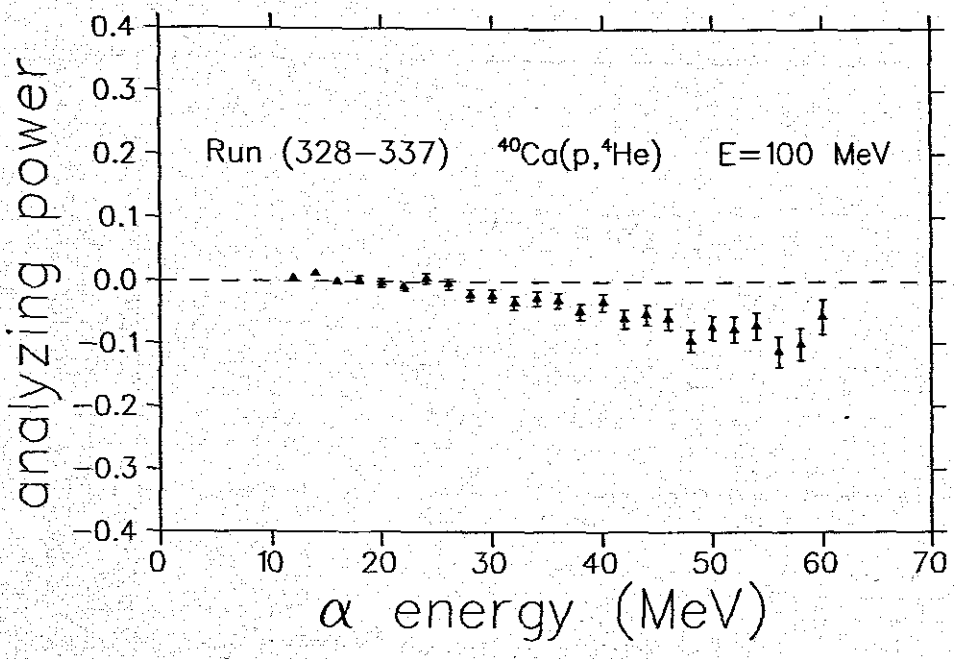

Figure 4.5: *Analyzing power results for weekend 4 taken at 40.12°. The error bars denote the statistical error of the measurement.*

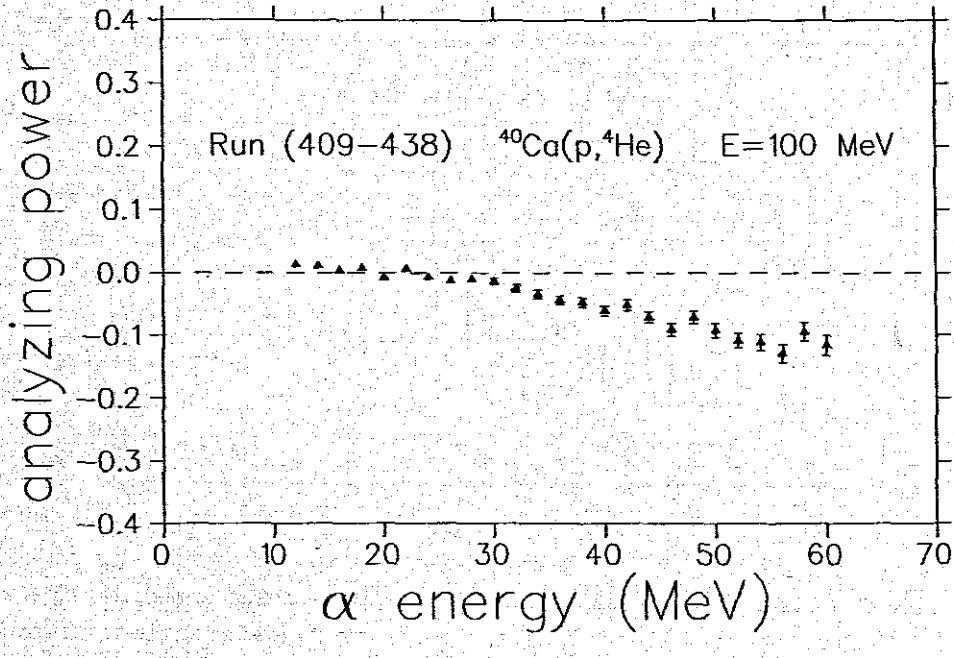

Figure 4.6: *Analyzing power results for weekend 5 taken at 40.12°. The error bars denote the statistical error of the measurement.*

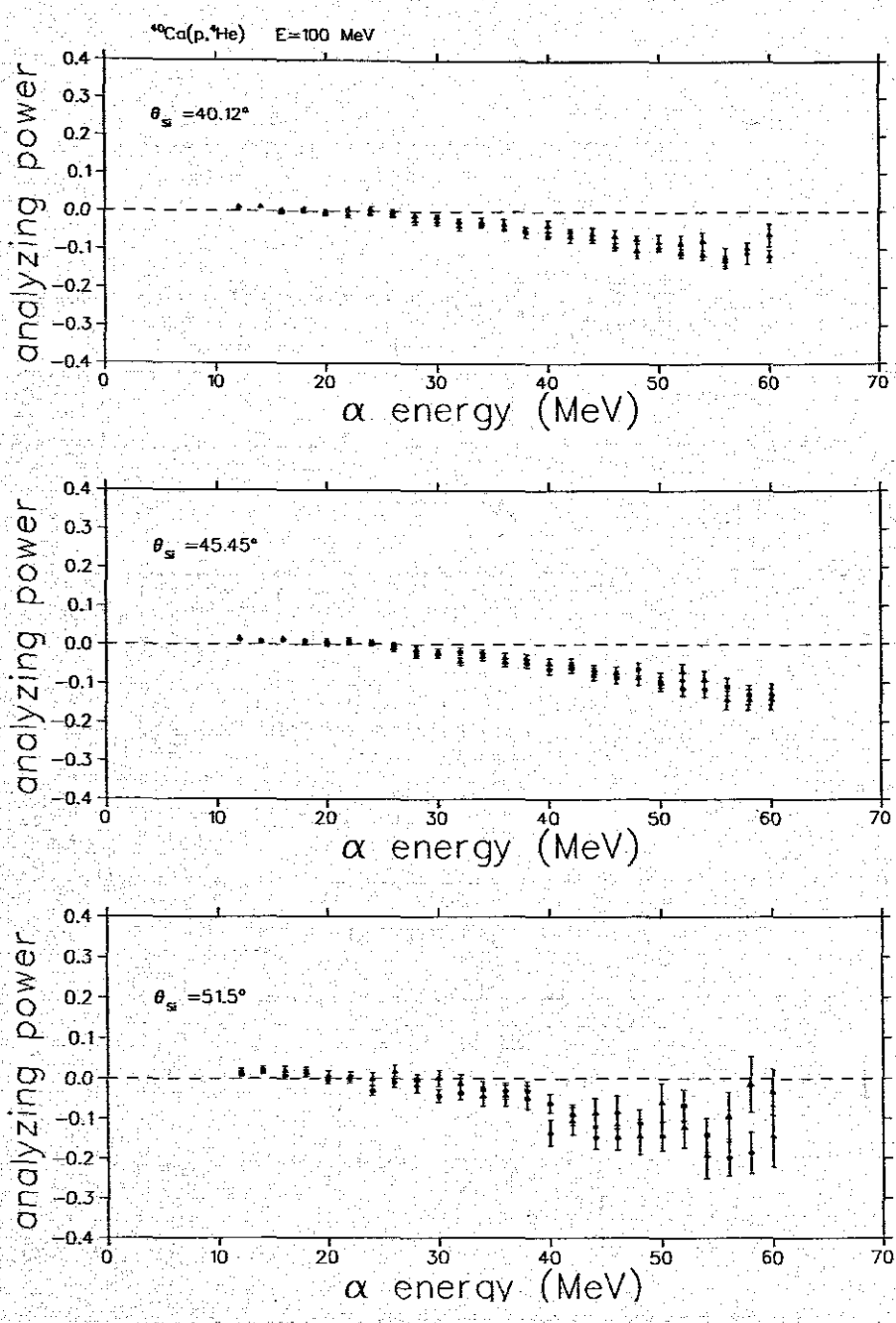

Figure 4.7: *Analyzing power results for all the weekends. The error bars denote the statistical error of the measurement.*

do not agree with the experimental data but the theory overestimates the experimental data. These results were plotted using PHYSICA.

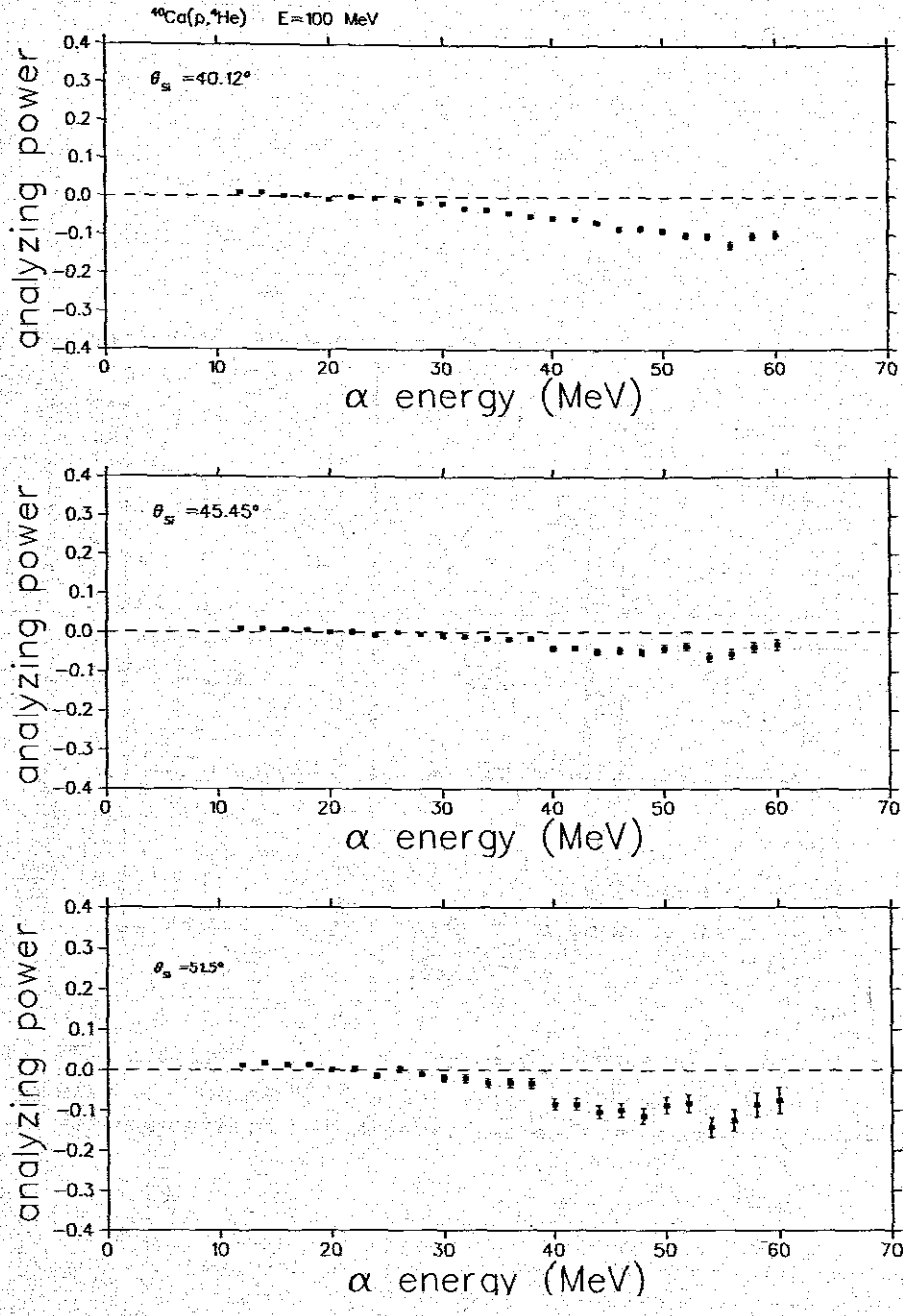

Figure 4.8: *Weighted mean analyzing power results for all the weekends . The error bars denote the statistical error of the measurement.*

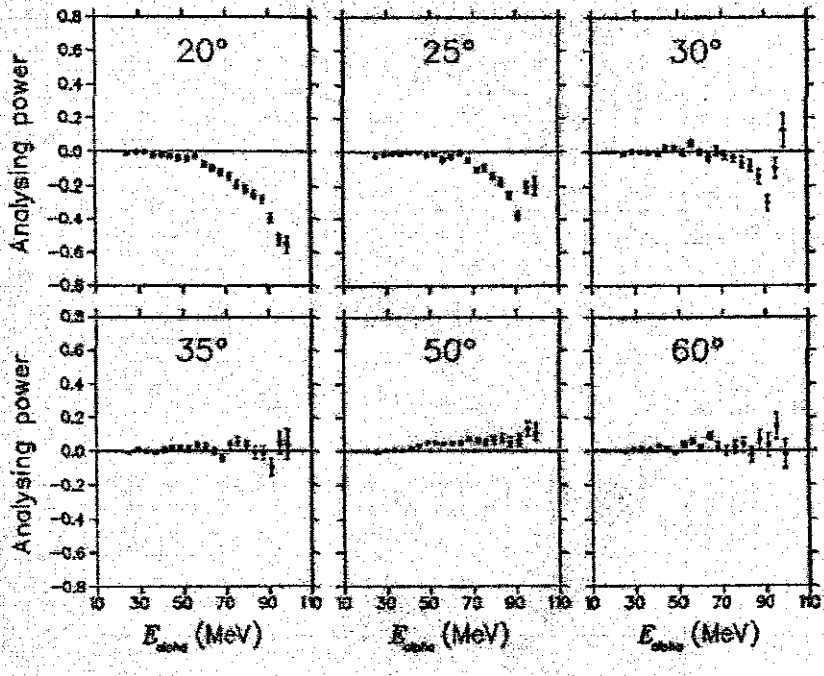

Figure 4.9: *^{59}Co analyzing power results measured from the pre-equilibrium emission in the (p,α)reaction on ^{59}Co and ^{93}Nb at an incident energy of 100 MeV. This results are taken from the progress report to PAC in the year 2000 by Cowley et al [Cow00]*

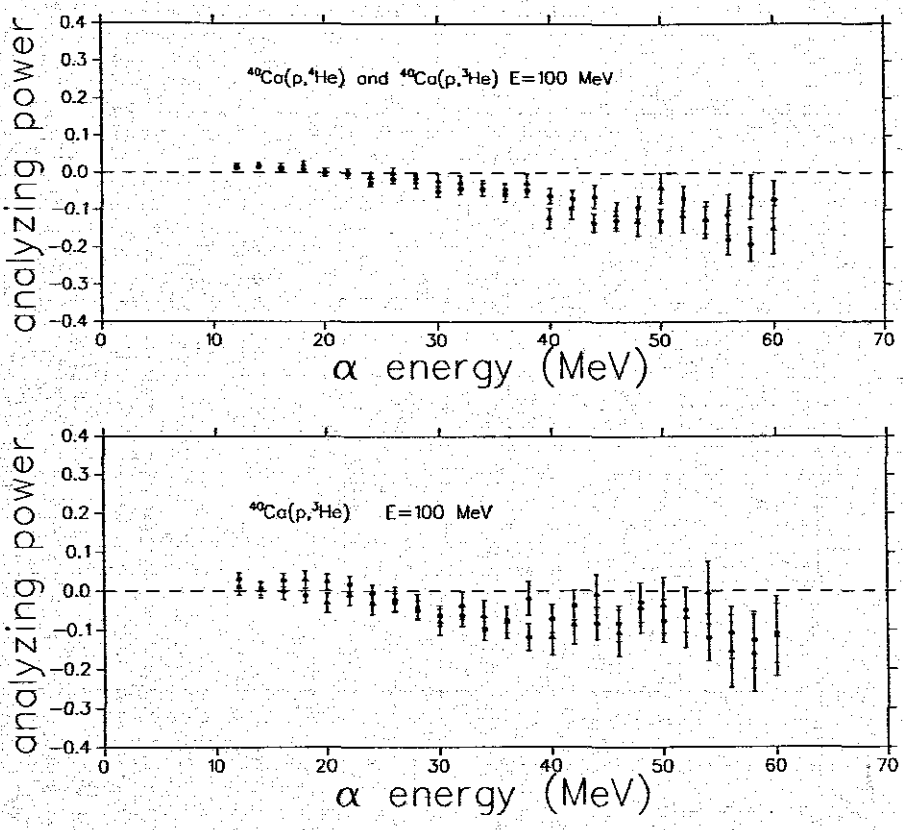

Figure 4.10: *Analyzing power results for ^{3}He for two different weekends (weekend 2 and weekend 3, triangles and circles respectively) and the results for ^{3}He (triangles) and ^{4}He (circles) together. The data was taken at 51.5°. The error bars denote the statistical error of the measurement.*

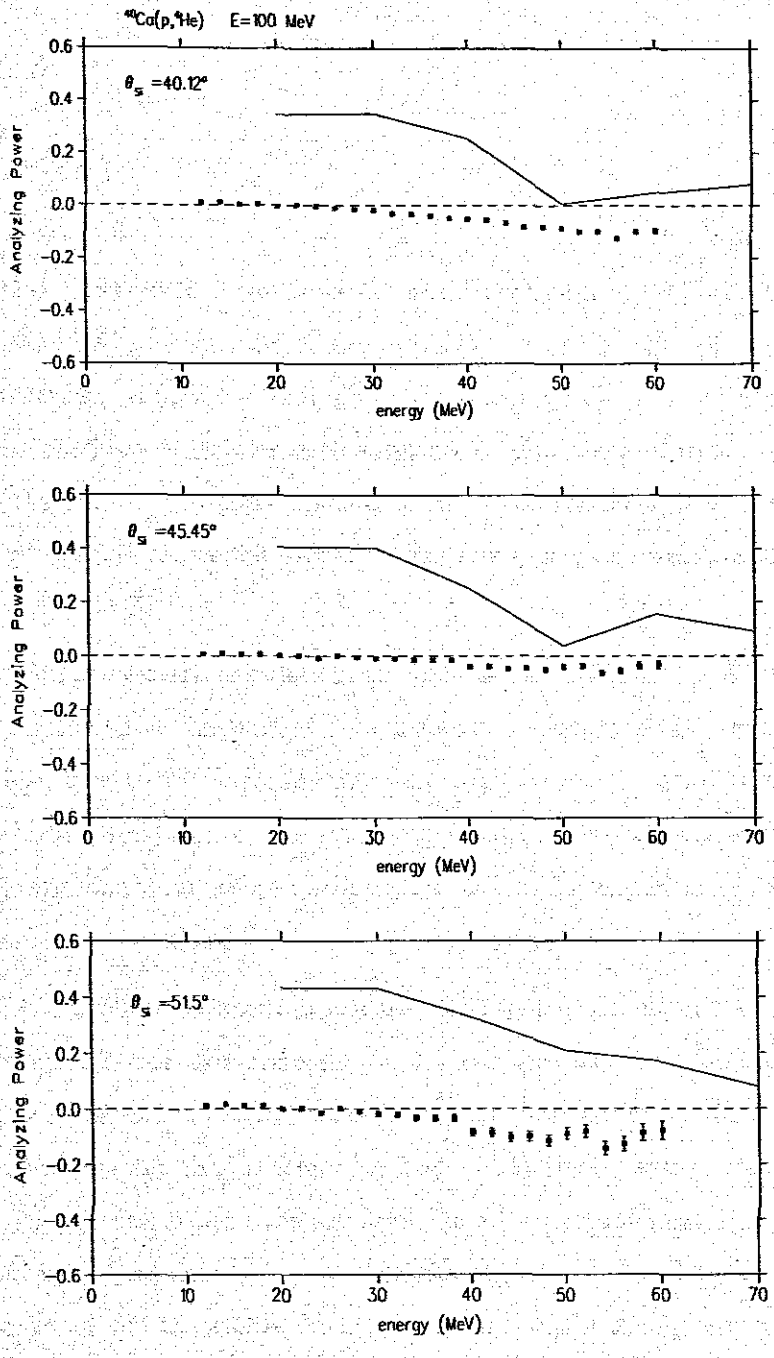

Figure 4.11: *A comparison between the experimental analyzing power solid squares and the theoretical analyzing powers solid curves for all the weekends. The error bars denote the statistical error of the measurement.*

Chapter 5

Conclusion

The focus of this study was to investigate the analyzing power of the inclusive ^{40}Ca$(\vec{p},\alpha)$ reaction at 100 MeV for different coplanar quasi-free angle pairs of the co-incidence $^{40}Ca(\vec{p},\alpha)$ reaction. The data analysis of the singles data helps to ensure that the quality of the coincidence data for each weekend is sufficient and that the results from the various datasets can be added together without compromising the quality of the final coincidence data. The second aspect of this study was to investigate the clustering phenomena.

The quality of the experiment data is good. This conclusion is based on the fact that the datasets for the same kinematics from different weekends of data taking agree well with each other. The trend for all the datasets agree very well with each other. i.e. the shape for each data set taken at the same angle is approximately the same. Moreover, these datasets are consistent within the statistical error. The experimental results suggest a multistep process since there are zero analyzing powers for each one of them.

The DWIA theoretical framework successfully predicts knockout reaction cross sections only for coincidence measurements for targets such as ^{40}Ca. The comparison between the theoretical and the experimental analyzing power distribution for the inclusive ^{40}Ca$(\vec{p},\alpha)$ measurement that is shown in Fig. (4.11) clearly shows that the theoretical analyzing power values are different from the experimental analyzing power values. Although the theoretical analyzing power results do not agree well with the experimental data, the trend for theoretical analyzing powers qualitatively agrees with that of the experimental analyzing power results. Moreover, theoretical analyzing power results overestimate the experimental analyzing power data. This could mean that the code (THREEDEE code) used was not suitable for the present data and consequently the the-

oretical model may not be correct. This might result from the interpolation since (p,^{4}He) elastic scattering data at 100 MeV - Q-value ($\approx$ 92.96 MeV) is not available.

Our data does not support the idea of preformed clusters in the ^{40}Ca nucleus. This is seen in the experimental analyzing power distributions with zero analyzing powers at low α energies and the negative (less than zero) analyzing powers at high α energies.

According to Cowley *et al.* [Cow02] direct knockout is expected to be associated with large analyzing power values. However in the experimental results of this study there are no substantial analyzing power values.

Bibliography

[Are97] G.J. Arendse, Ph.D. thesis, University of Stellenbosch, (1997), unpublished.

[Bau98] E. Bauge, J.P. Delaroche and M. Girod, *Phys. Rev.* **C58** (1998) 1118.

[Ber62] T. Berggren, G.E. Brown, G. Jacob, *Phys. Lett.* **1** (1962) 88.

[Ber73] F.E. Bertrand and R.W. Peelle, *Phys. Rev.* **C8**, (1973) 1045.

[Ber77] W. Bertozzi, M.V. Hynes, C.P. Sargent, C. Cresswell, P.C. Dunn, A. Hirsch, M. Leitch, B. Norum, F.N. Rad and T. Sasanuma, *Nucl. Instrum. Methods* **141** (1977) 457.

[Bon89] R. Bonetti, F. Crespi and K. Kubo *Nucl. Phys.* **A499** (1989) 381.

[Bri73] D. Brink, Castro J.J. *Phys. Rev* **A216** (1973) 109.

[Car84] T.A. Carey *et al.*, *Phys. Rev.* **C29** (1984) 1273.

[Car99] T.A. Carey *et al.*, *Phys. Rev.* **A649** (1999) 57.

[Chr78] R.E. Chrien *et al.* Winnipeg Conference (1978) 628.

[Cow96] A.A. Cowley, G.J. Arendse, J.W. Koen, W.A. Richter, J.A. Stander, G.F. Steyn, S.S. Dimitrova, P.E. Hodgson, Y. Watanabe, *Phys. Rev.* **C54** (1996) 778.

[Cow97] A.A. Cowley, G.J. Arendse, W.A. Richter, J.A. Stander, G.F. Steyn, S.S. Dimitrova, P. Demetriou, P.E. Hodgson, *Phys. Rev.* **C55** (1997) 1843.

[Cow02] A.A. Cowley, S.V. Förtsch, G.F. Steyn, S.S. Dimitrova, P.E. Hodgson, *Phys. Rev.* **C54** (2002) 742.

[Cow00] A.A. Cowley, G.F. Steyn, S.S. Dimitrova, P.E. Hodgson, G.J. Arendse, S.V. Förtsch, G.C. Hillhouse, J.J. Lawrie, R. Neveling, W.A. Richter, J.A. Stander, and S.M. Wyngaardt et al., *Phys. Rev.* **C62** (2000).

[Cow00] A.A. Cowley, G.F. Steyn, S.S. Dimitrova, P.E. Hodgson, G.J. Arendse, S.V. Förtsch, G.C. Hillhouse, J.J. Lawrie, R. Neveling, W.A. Richter, J.A. Stander, and S.M. Wyngaardt, PAC progress report, (2000).

[Gre82] Ray E.L. Green, K. Peter Jackson, and Ralph G. Korteling *Phys. Rev.* **C25** (1982) 828.

[Hod03] P.E. Hodgson and E. Betak, *Physics Reports* **374** (2003) 1.

[Hod97] P.E. Hodgson, E. Gadioli and E. Gadioli Erba, *Introductory nuclear physics*, Oxford University Press, (1997).

[Hod94] P.E. Hodgson *et al.*, *Z. Phys. Rev.* **A349**, (1994) 197.

[Jac66] G. Jacob and A.J. Maris, *Rev. Mod. Phys.* **38** (1966) 121.

[Kit85] P. Kitching, WJ McDonald, Th. AJ Maris and CAZ Vasconcellos, Advances in Nuclear Physics, ed. JW Negele and E. Vogt, Vol. 15 (Plenum, New York,1985) 43.

[Kra87] Kenneth S. Krane, *Introductory Nuclear Physics*, Wiley, (1987) 457.

[Leo87] W.R Leo, *Techniques for Nuclear and Particle Physics Experiments*, Springer Verlag, Berlin (1987) 90.

[Nad80] A. Nadasen *et al.*, *Phys. Rev.* **C22** (1980) 1394.

[Nad81] A. Nadasen *et al.*,*Phys. Rev.* **C23** (1981) 2353.

[Nad89] A. Nadasen *et al.*, *Phys. Rev.* **C40** (1989) 1130.

[Nad89] P.G. Roos, N.S. Chant, C.C. Chang, G. Ciangaru, H.F. Breuer, J. Wesick, *Phys. Rev.* **C40** (1989) 1130.

[Nad81] A. Nadasen *et al.*, *Phys. Rev.* **C23** (1981) 2353.

[Nad83] A. Nadasen *et al.*, *IUCF Scientific and Technical Report*, (1983), p13.

[Nad99] A. Nadasen *et al.*, *Phys. Rev.* **C59** (1999) 760.

[Nev98] R. Neveling, Master's Thesis, University of Stellenbosch, (1998).

[Nev01] R. Neveling, PhD Thesis, University of Stellenbosch, (2001).

[Nev04] R. Neveling, experiment proposal, iThemba LABS, (2004).

[Nev05] R. Neveling, private communication, iThemba LABS, (2005).

[Pil96] J.V. Pilcher, *The NAC MBD to VME Conversion Guide*, National Accelerator Centre, (1996)(unpublished).

[Ren91] E. Renshaw, S.J. Yennello, K. Kwiatkowski, R. Planeta, L.W. Woo, and V.E. Viola, *Phys. Rev.* **C44**, (1991) 2618.

[Roo77] P.G. Roos *et al.*, *Phys. Rev.* **C15** (1977) 69.

[Stey99] G.F. Steyn *et al.*, *Phys. Rev.***C59** (1999) 2097.

[Wan85] C.W. Wang *et al.*, *Phys. Rev.* **C31** (1985) 1662.

[Yos98] T. Yoshimura *et al.*, *Nucl. Phys.* **A641** (1998) 3.